THESIS

# A FRAMEWORK FOR SIMULTANEOUS PHOTON DETECTOR READOUT SYSTEM SIMULATIONS FOR THE DEEP UNDERGROUND NEUTRINO EXPERIMENT


Submitted by

Anne R. Christensen

Department of Physics


In partial fulfillment of the requirements

For the Degree of Master of Science

Colorado State University

Fort Collins, Colorado

Summer 2020

Master's Committee:

Advisor: Norm Buchanan

Kate Ross
Wolfgang Bangerth

ABSTRACT

A FRAMEWORK FOR SIMULTANEOUS PHOTON DETECTOR READOUT SYSTEM SIMULATIONS FOR THE DEEP UNDERGROUND NEUTRINO EXPERIMENT

This thesis will discuss the changes to the coding framework for the Deep Underground Neutrino Experiment (DUNE). DUNE is simulated in a coding framework, called Liquid Argon Software (LArSoft). The framework simulates the particle event, the photons produced due to interactions and the electronics. The electronic simulation framework for DUNE has been changed to improve functionality and ease of use. The electronics simulation has been modularized so electronic readout models can be directly compared. The changes to the framework will be described and validated in this thesis.

ACKNOWLEDGEMENTS

I would like to thank my advisor, Professor Norm Buchanan, for his support in this thesis and my work for DUNE. His help has been invaluable to me. I would, also, like to thank the DUNE collaboration, specifically those I have worked with on this, Alex Himmel, Kate Scholberg and Jason Stock, who have answered my questions about the simulation. I would like to thank my committee, Professor Kate Ross and Professor Wolfgang Bangerth, for agreeing to read through this thesis and give me their comments.

Additionally, I would like to thank the CSU Lab, and my colleagues there, including Jay Jablonski and David Warner, for taking the time to teach me about the electronics and hardware involved with the experiments.

## DEDICATION

*I dedicate this to my family and thank them for all their support.*

TABLE OF CONTENTS

LIST OF FIGURES

LIST OF ACRONYMS

**ADC** Analog to Digital Converter.

**APA** Anode Plane Assembly.

**CP** Charge Parity.

**CPA** Cathode Plane Assembly.

**DBR** Dynamic Bit Range.

**DUNE** Deep Underground Neutrino Experiment.

**FBK** Fondazione Bruno Kessler.

**LAr** Liquid Argon.

**LArSoft** Liquid Argon Software.

**LArTPC** Liquid Argon Time Projection Chamber.

**PDS** Photon Detection System.

**pTP** p-TerPhenyl.

**QDC** Charge Integration.

**SiPM** Silicon Photomultiplier.

**SNO** Sudbury Neutrino Observatory.

**SSP** SiPM Signal Processor .

**SURF** Sanford Underground Research Facility.

**TPB** Tetra-phenyl Butadiene.

**TPC** Time Projection Chamber.

# Chapter 1

# Introduction

Neutrinos are very small, very light particles. They are produced in the Sun, supernovae and by various other processes in the universe. Neutrinos only interact through the weak force, meaning they interact very rarely with other particles. As a result, neutrinos are extremely difficult to measure. Fortunately, neutrinos are very common in the universe and on Earth. Various experiments, such as the Deep Underground Neutrino Experiment (DUNE), aim to discover more about neutrinos and other exotic particles.

The Deep Underground Neutrino Experiment (DUNE) is a planned large, off-axis neutrino experiment. DUNE uses a neutrino beam originating at Fermilab, which will be the most intense neutrino beam in the world. The neutrino beam will be characterized by the near detector, located 210 m from the neutrino beam. After travelling 1300 km, the neutrino beam will be measured in the far detector, located 1.5 km underground at the Sanford Underground Research Facility in Lead, South Dakota. The far detector consists of two main components: the Liquid Argon Time Projection Chamber (LArTPC) and the Photon Detection System (PDS). The LArTPCs will measure the charge deposited by a particle as it passes through the detector. The Photon Detection System will measure the photons produced from particle interactions in the detector. The electronics will record the data from the two systems [3].

The DUNE experiment is simulated in a software framework, called Liquid Argon Software (LArSoft), that simulates the neutrino beam and detectors. The code simulates the electronic signal from the LArTPC, the electronic response, and the photon signals from the PDS. My work involved modularizing the electronic readout simulation for the PDS in order to allow more flexibility. An electronic readout model digitizes the photon signals from the PDS. Before the changes, only one type of electronic readout model could be simulated. Following the changes, multiple electronic readout models can be simulated and compared directly. Dark noise, detector efficiency, cross talk, line noise and the waveform digitization were restructured in the simulation, allowing for a modular framework. In addition, my work involved implementing saturation into the simulation. The electronic simulation was tested rigorously to determine that the changes did not change the simulated data [10].

# Chapter 2

# Motivation And Neutrino Physics

## 2.1 Motivation

During a supernova, massive amounts of neutrinos are produced through electron capture. Electron capture begins when heavy nuclei capture free electrons, resulting in electron neutrinos. Thus far, the only neutrino flux measured from a supernova came from SN 1987A, in 1987. The neutrinos from SN 1987A put loose limits on the mass of the neutrino and gave insight into supernovae processes. However, even with information from the SN 1987A neutrinos, the core collapse mechanism of a supernova is not fully understood. Neutrinos from supernova events are typically low energy, on the order of 5 MeV to 100 MeV. To measure low energy neutrinos, the Photon Detection System (PDS) in DUNE is necessary. The PDS improves spatial, time and energy resolution within the detector. The photons are measured by the PDS on the order of nanoseconds after the interaction, improving the timing resolution. Energy resolution is improved using calorimetry of photons from interactions [11].

Additionally, proton decay is predicted by grand unified theories and is therefore of interest to physics. Proton decay is a very rare event, with a predicted decay lifetime of greater than $10^{33}$ years. If proton decay occurs, then the detector must measure it with certainty. If a proton decays, the PDS measures the photons from the decay and triggers storage of the event [3].

## 2.2 Neutrino Physics

Pauli initially predicted neutrinos in 1930 to solve the issues with energy and momentum conservation in $\beta$-decay [12]. $\beta$-decay ($p \to n + \nu + e^+$) is the radioactive decay of an atom which emits an electron or positron. A common form of $\beta$-decay is the decay of carbon-14 into nitrogen-14 and a positron. When studying the decay, there was 'missing energy'. Either conservation of energy was violated, or another particle must exist. As a result, the neutrino was theorized as a nearly undetectable particle, meaning it must be small, neutral, and very weakly interacting.

Fortunately, neutrinos are plentiful in the universe. On Earth, about 100 billion solar neutrinos pass through a person's thumbnail each second. These Solar neutrinos reach Earth and create a background for detectors. However, on average, the majority of neutrinos that reach Earth pass through without interacting with a single particle. Fortunately, neutrinos are very abundant in the universe. In fact, a typical nuclear reactor has a neutrino flux of about $10^{11}$ $\nu/\text{cm}^2/\text{s}$ only meters away from the core. Neutrinos interact very weakly, and detectors only measure a small portion of the neutrinos which pass through the detector [1].

Reines and Cowan used this fact, along with inverse beta decay ($\bar{\nu} + p \rightarrow n + e^+$), to detect anti-neutrinos [13]. Inverse beta decay results in a positron and neutron, both of which are measurable particles. Reines and Cowan reduced backgrounds in the experiment by comparing the timing of the measurement of the positron and neutron in the detector.

After the confirmation of the neutrino, experiments were devised to develop a neutrino beam for more detailed study. During this time, neutrino flavors were also discovered, that is $\nu_\mu$, $\nu_e$ and $\nu_\tau$ with their corresponding, massive leptons $\mu$, $e^-$, and $\tau$. Pion decay ($\pi^- \rightarrow \mu^- + \bar{\nu}_\mu$) was discovered and became a starting point for neutrino beam physics [1].

The first accelerator neutrino beam, built in 1962 by Lederman, Schwartz and Steinberger, produced a proton beam that was directed into a target, as shown in Fig 2.1. The protons collide with the neutrons and protons in the target, creating pions and kaons. Pions and kaons primarily decay into neutrinos, electrons and muons. The muons and electrons are blocked by 13.5 m of steel and concrete shielding so only neutrinos remained [14].

Futhermore, the Davis experiment measured the solar neutrino flux and introduced the solar neutrino problem. The Davis experiment used inverse $\beta$-decay, $\nu_e +^{37} Cl \rightarrow^{37} Ar + e^-$, to capture neutrinos in a tank filled with $^{37}Cl$. The number of solar neutrinos measured were only a third of the predicted number, indicating neutrino oscillation [15]. Further measurements at

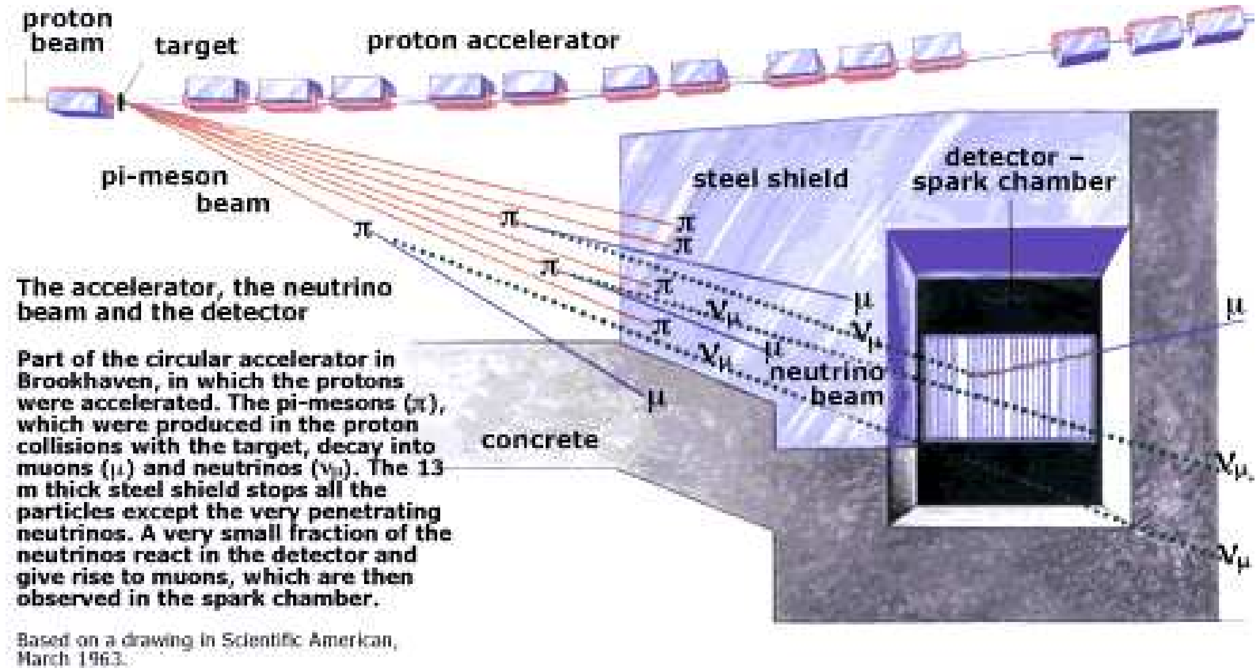


**Figure 2.1:** The Lederman, Schwartz and Steinberger experimental setup, including the proton beam, shielding and detector [1].

Sudbury Neutrino Observatory (SNO) [16] and Super Kamiokande [17] demonstrated that neutrinos change flavor between $\nu_\mu$, $\nu_e$ and $\nu_\tau$. Because neutrinos oscillate, they must have mass.

Neutrinos can be described by mass and flavor states. The flavor states are unitary combinations of the mass states, meaning that the flavor states can be defined in terms of a combination of the mass states.

At the beginning of the universe, matter and anti-matter were created equally. Now, matter is much more common than anti-matter. Therefore, some symmetry rules for particle interactions must be broken. Charge conjugation symmetry is the main concern for matter and anti-matter. Charge conjugation symmetry relates to the result of conjugating quantum numbers including electric charge, baryon number, and lepton number. Matter and anti-matter particles have the same mass but opposite quantum numbers. However, charge conjugation symmetry is not violated. There is evidence of Charge-Parity (CP) violation, which is a combination of charge conjugation symmetry and parity symmetry.

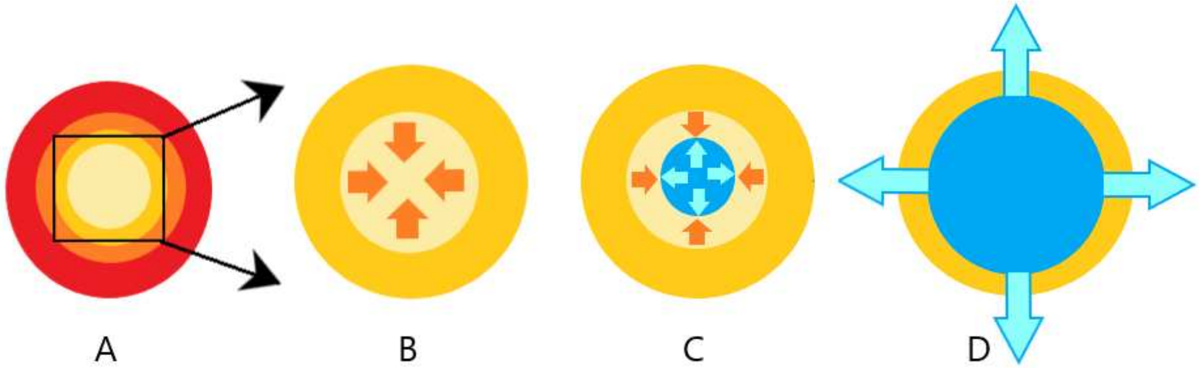


**Figure 2.2:** (A) The star is fully evolved with an iron core. (B) The core of the star is no longer supported by fusion and the star falls inward to create a neutron center which can no longer collapse. Neutron degeneracy pressure causes the core to rebound outwards, creating a shockwave. (C) The shockwave stalls. (D) After a small amount of extra energy from the neutrinos adds to the shockwave, the shockwave continues outward, and the supernova commences.

Parity symmetry is the concept that the mirror image of a particle interaction is possible. While this is true in electromagnetic and strong force interactions, parity symmetry does not always hold in weak interactions. Charge-Parity (CP) violation combines the two symmetries. Since the two symmetries are connected, CP violation for neutrinos and anti-neutrinos could explain the asymmetry of matter and anti-matter. CP violation can be measured through neutrino oscillations [18].

The scope of my research focuses on low energy interactions in the Deep Underground Neutrino Experiment (DUNE), Chapter 3, which includes supernova neutrinos and proton decay. The focus of this thesis is on building and testing a framework for electronic simulation of the Photon Detection System.

## 2.3 Supernova Neutrinos

Type II supernovae occur when massive stars from 8 solar masses to 50 solar masses undergo a core collapse. Above 50 solar masses, the star collapses into a black hole. This results in an explosion, which ejects a burst of neutrinos on order of $10^{58}$ [11]. A supernova will proceed differently depending on the mass of the star. A star will evolve until its core becomes iron. Once fusion is not energetically favorable, gravity will cause the star to undergo core collapse.

A supernova core collapse begins with each of the shells of the star burning and the core contracting. A succession of nuclear reactions occur as a result. Toward the end of these nuclear reactions, the star reaches a very high temperature. At this point, photons have enough energy to knock out subatomic particles from nuclei, a process called photodisintegration [19].

Heavy nuclei begin to capture electrons; a phenomenon called electron capture. This process results in electron neutrinos through the interaction $p^+ + e^- \rightarrow n + \nu_e$. As this process continues, the core can no longer sustain itself and collapses, with particles in the core reaching nearly 70,000 km/s (about 25% the speed of light). After the density in the core exceeds $8 \times 10^{17}$ kg/m$^3$, the neutron degeneracy pressure causes the core to rebound outwards. These waves of pressure can create a shockwave. However, as the shockwave expands, photodisintegration begins again, slowing the shockwave. At this point, the shockwave will stall. However, the density is so large that neutrino scattering deposits some energy (about 5%) into the shockwave. The energy forces the shockwave to continue, resulting in a supernova [19].

In 1987, a star 51 kpc away in the Large Magellanic Cloud collapsed, becoming the supernova known as SN 1987A. During a period of 13 seconds, 25 neutrino events were observed in two water Cherenkov detectors and a liquid scintillator detector. Cherenkov detectors measure small particles using Cherenkov radiation, which is the process where a particle moves faster than the speed of light through a medium, creating a wave of light, similar to a sonic boom. Even with poor statistics, the neutrino events from SN 1987A gave insight to the limits of the cooling mechanisms of the particles emitted from supernova core and on various exotic neutrino properties, including decays and neutrino charge [11].

Supernova neutrinos are low energy (typically between 5 MeV and 100 MeV), as shown in Fig. 2.3, and nearby supernova events are rare, on order of one supernova each century per galaxy [11]. The Photon Detection System (PDS) can be used to correct the energy and as a trigger when events such as these happen. The photons move through liquid argon much faster than charged particles from interactions. As a result, the timing resolution can be improved and the time of the event, $t_0$, can be found more accurately. Information about $t_0$ leads to in-

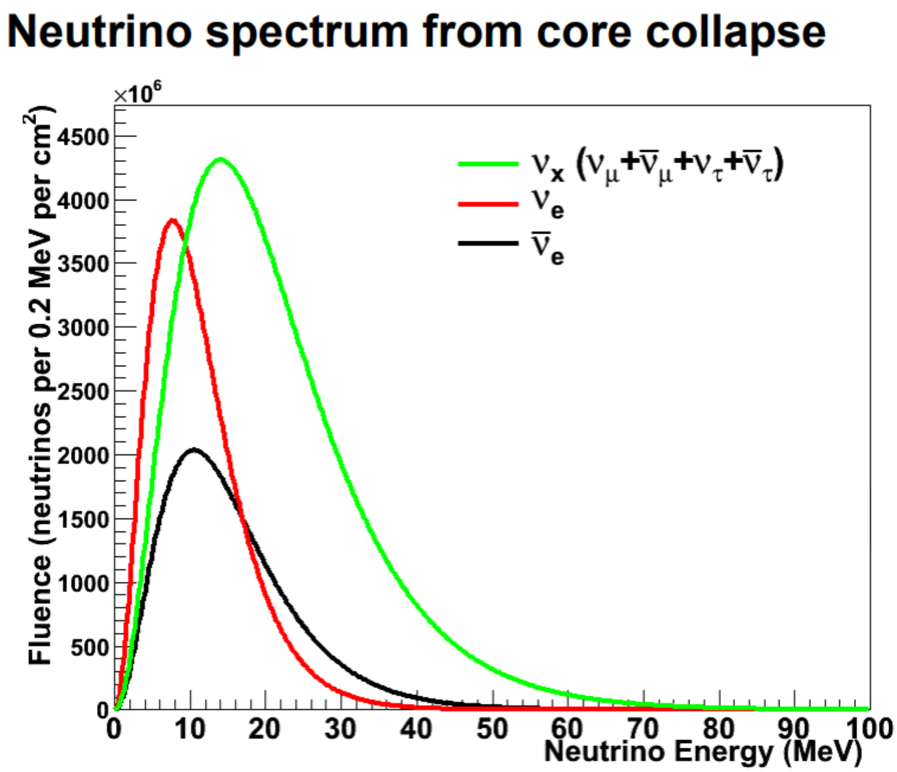


**Figure 2.3:** The predicted neutrino spectrum from a supernova core collapse [2].

formation about the precise position of the particle in the detector. As a particle moves through the detector, energy is deposited within the detector. Therefore, the energy deposited depends on the initial location of the particle in the detector.

# Chapter 3

# The Deep Underground Neutrino Experiment (DUNE)

The Deep Underground Neutrino Experiment (DUNE) is being designed to search for Charge-Parity (CP) violation, mass hierarchy, proton decay, and supernovae neutrinos, as well as other physics. Charge-Parity (CP) violation could explain the matter and anti-matter asymmetry throughout the universe, as discussed in Sec. 2.2. Proton decay and supernova neutrinos require the Photon Detection System (PDS) in DUNE. Photons from proton decay and supernova neutrinos are measured by the PDS, which indicate that the event should be stored. Additionally, the PDS is necessary for low energy events since these events need improved energy resolution.

The Deep Underground Neutrino Experiment (DUNE) is a proposed long-baseline, off-axis neutrino experiment consisting of a high-power neutrino beam, a near detector and a far detector. The neutrino beam originates at Fermilab, near Chicago, and is directed toward the far detector nearly 1300 km away. The DUNE neutrino beam will be the world's most powerful, with an initial power of 1.2 MW. The near detector will be located 575 m from the neutrino source and will be used to characterize the beam and aid in minimizing beam-related systematic uncertainties [3].

To create the beam, protons are accelerated to 80 GeV and collide with a graphite target. Mesons, largely pions and kaons, are created by the protons when they collide with the target. The mesons are then directed through a 200 m decay pipe, where they decay into neutrinos and other particles. Any remaining mesons are removed from the beam with a thick layer of concrete and steel at the end of the decay pipe, resulting in a pure neutrino beam. While all flavors of neutrinos are created in this process, the majority of the neutrinos are muon neutrinos [20].

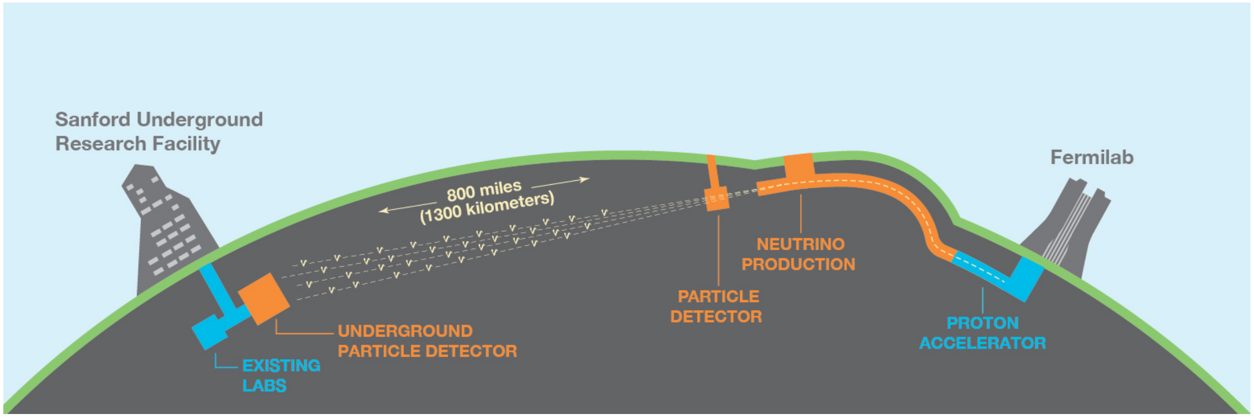


**Figure 3.1:** The location and setup of the detectors and beam involved in DUNE [3].

The far detector is located in South Dakota at the Sanford Underground Research Facility (SURF) and will be located about 1.5 km underground. The detector uses Liquid Argon Time Projection Chamber (LArTPC) technology to measure events within the detector. The active part of the detector (fiducial) has a mass of 40 kt. LArTPCs creates detailed images of the particle paths. Additionally, the far detector includes a photon detection system to measure light resulting from interactions in the detector [5].

DUNE is designed to precisely measure neutrino oscillation parameters, including the charge parity (CP) violating phase, neutrino mass ordering, and the mixing angle $\theta_{23}$. The CP-violating phase measurement is a measure of CP violation in neutrino interactions.

Another goal of the DUNE experiment is to observe proton decay since this is a key element in grand unification theories. Additionally, DUNE can be used to measure neutrinos from a supernovae. During the core collapse of supernova, neutrinos are created in large quantities and galactic supernovae will result in hundreds to thousands of neutrino events in the DUNE far detector. Only one supernova resulted in neutrinos being detected in neutrino particle detectors. DUNE will provide insight into supernovae physics by measuring the neutrino flux from any galactic supernovae occurring during its operation.

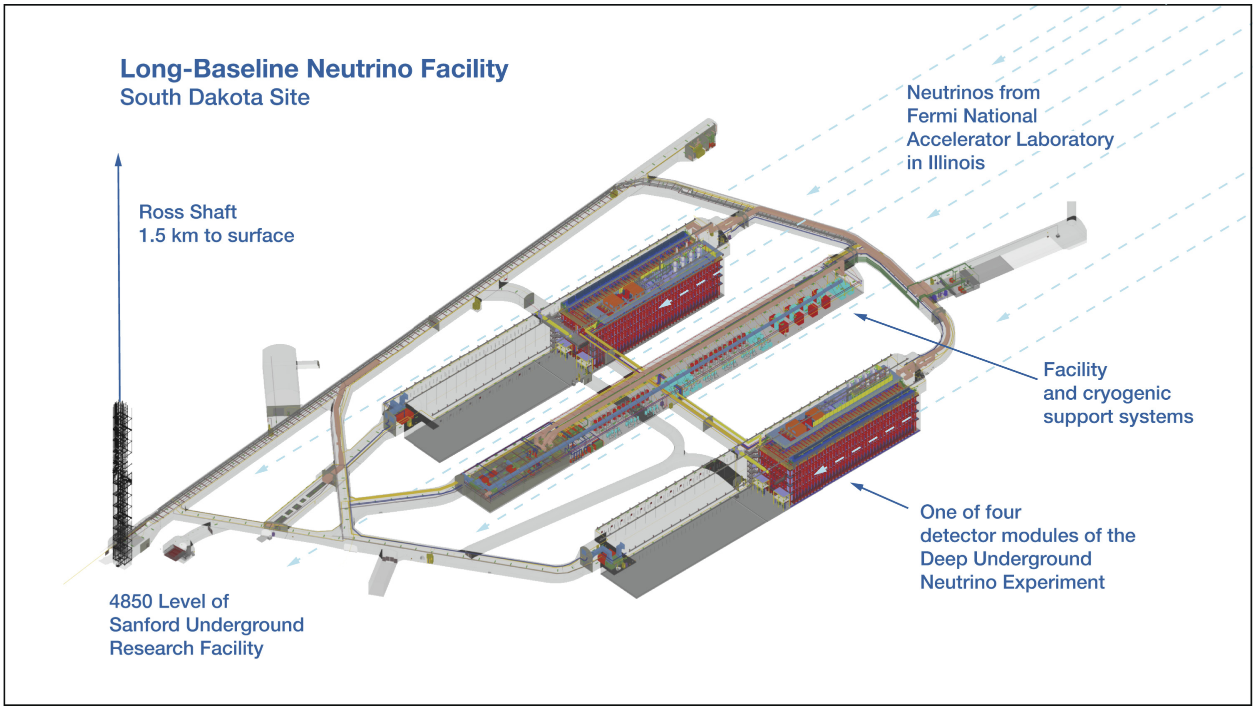


**Figure 3.2:** The future DUNE far detector complex, located in South Dakota at SURF [4].

## 3.1 Far Detector Design

The far detector is designed to measure charged particles resulting from interactions within the detector. DUNE's far detector, shown in Fig. 3.2, is proposed to have four detector modules, a combination of single phase and dual phase modules. The single phase modules use liquid argon, while the the dual phase uses both liquid and gaseous argon in stages. Each single phase module consists of an active mass of 10 kt of Liquid Argon, 6000 photon detection channels, and 150 anode plane assemblies. A voltage is applied across the Liquid Argon to move the charged particles to the detector. The far detector measures energy of the particles, the charge of the particles, and the photons produced from the particle interactions when the ionized atoms recombine.

When particles interact inside the Liquid Argon (LAr) toward the anode, the interactions ionize the Argon, resulting in free electrons. The electrons drift in the Time Projection Chamber (TPC) and the charge is collected. The TPC consists of sets of Anode Plane Assemblies (APAs) and Cathode Plane Assemblies (CPAs). The CPAs are held at -180 kV and the APAs are grounded to achieve 500 V/cm in the volume within the chamber [5].

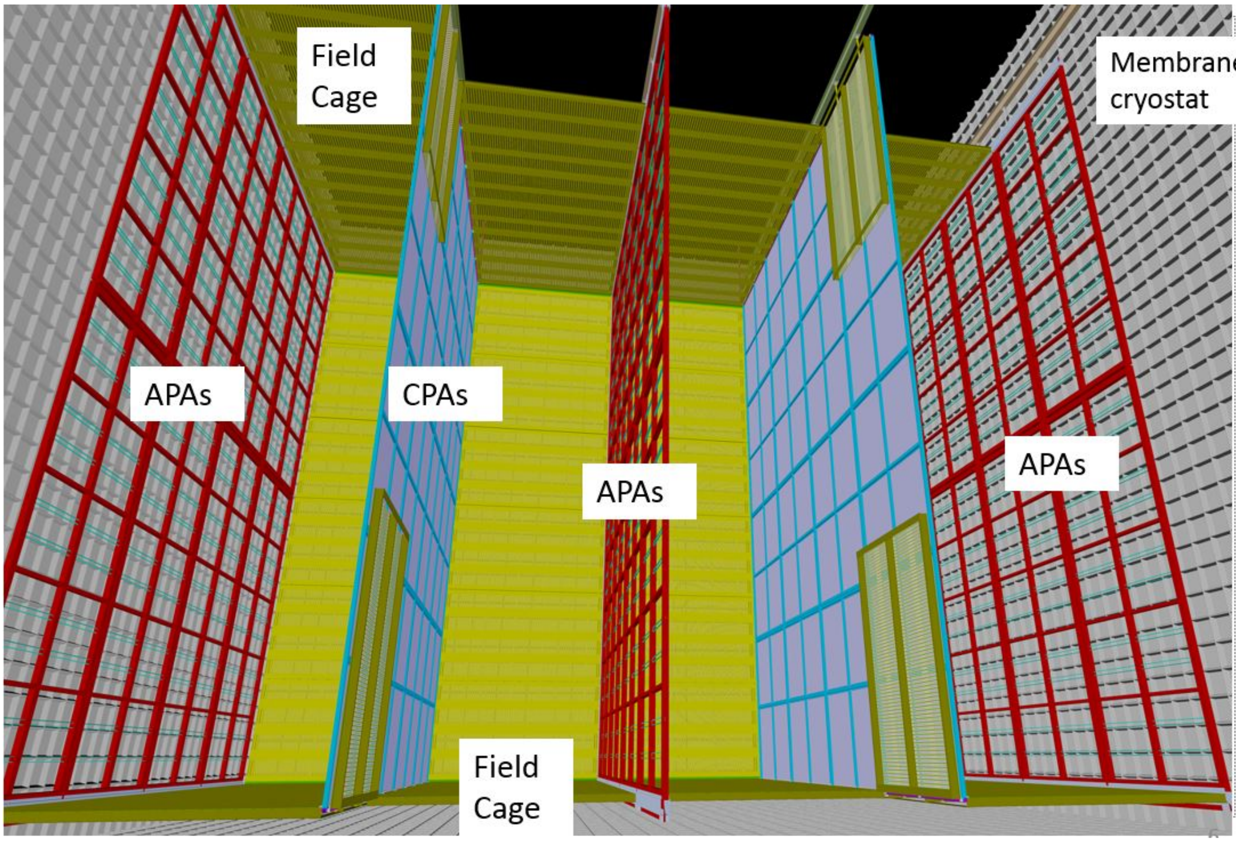


**Figure 3.3:** A slice of the Time Projection Chamber showing the CPA and APA setup [5].

Each APA is 6 m high and 2.3 m wide and is covered with 2500 sense wires. The sense wires are arranged into three planes, a vertical collection plane, and two induction planes at an angle of ±35.7° to the vertical in the X-Y plane. The induction planes are angled such that each wire on one plane only crosses a given collection wire at one point. This scheme removes ambiguity as to the position of the electron. The vertical (X) and horizontal (Y) position on the APA is found from the wires through knowing where the induction wire and collection plane wire crosses. The position of the electron between the CPA and APA (Z) is found using knowledge of $t_0$, discussed further in the next paragraph. The three planes enable multi-dimensional reconstruction of the particle's path through the detector, shown in Fig. 3.4.

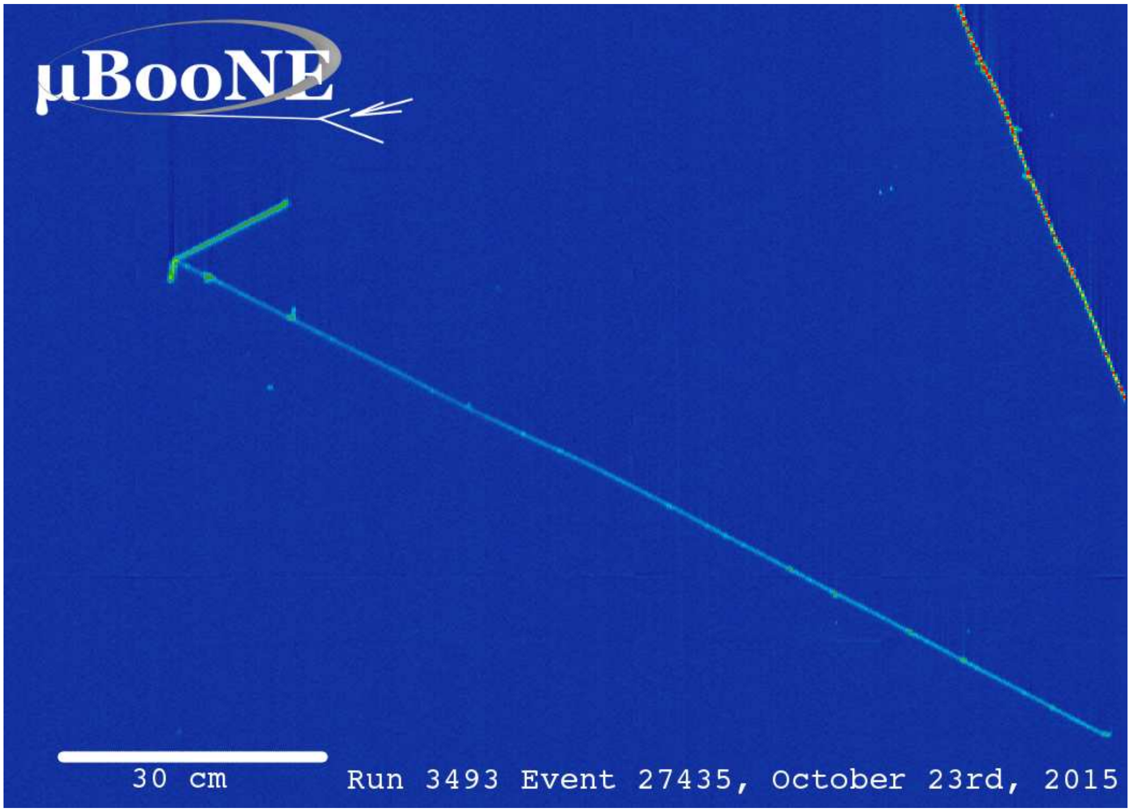


**Figure 3.4:** A neutrino event shown in the MicroBooNE detector [6].

The electrons drift from the CPAs to the APAs. The maximum drift length is 3.53 m, which determines the time resolution. As electrons drift, they can interact with other atoms or be reabsorbed by impurities in the liquid argon. The electron's interactions with the impurities results in energy loss. The PDS improves resolution for the time of the event, $t_0$, from a timing resolution on the order of milliseconds to nanoseconds. Therefore, the initial location of the electron in the detector is known better and the energy loss can be corrected in analysis. Additionally, the high voltage difference reduces the chance of recombination with the liquid argon [5].

# Chapter 4

# Photon Detection System

The Photon Detection System (PDS) is used to measure scintillation light resulting from particle interactions within the LArTPCs. The PDS enables accurate determination of the start time of events. Knowing the timing of the event is primarily necessary for events in the wild, such as proton decay and supernova neutrinos and can help reduce backgrounds originating outside of the detector. Events from the neutrino beam have a known timing, since the beam is pulsed. The TPC drift length is 3.53 m, with a drift time on the order of several milliseconds [5].

Improved timing resolution enables much more precise localization of events, on the order of millimeters, within the volume of the LArTPC, which is required for the full suite of DUNE physics. The timing is important for determining the energy of the particles since less charge is deposited on the APAs when the particles drift farther distances due to scattering as the electrons drift across the LAr volume. Additionally, there may be nonuniform portions within the detector, such as a broken resistor in a CPA which creates a nonuniform electric field. Knowing the localization of the event allows for the correction of energy to improve reconstruction of the event [5].

Raw data from the detector is sizable, with 6 GB per far detector module per 5.4 ms readout window. This amount of data is impossible to analyze by hand. Therefore, DUNE uses triggers, which determine important events in the detector. The PDS can be used as a trigger for non-beam events like supernova neutrinos or a proton decay event. The PDS can improve calorimetry measurements, in combination with charge measurements from the APAs, to improve energy resolution. Calorimetry is especially useful for low energy events, such as those from supernovae [5].

The scintillation photons produced by these events in the LArTPC are narrowly distributed around wavelengths of 127 nm in the vacuum ultraviolet. Therefore, the PDS must shift the photons to wavelengths more easily measured by photosensors [5].

The PDS is made up of four main components: wavelength-shifters, optical reflection or transport components depending on the design, Silicon Photomultipliers (SiPMs), and readout electronics [5].

## 4.1 Wavelength Shifters

Wavelength-shifters are chemicals that change the wavelength of light. There are two chemicals considered for DUNE, tetra-phenyl butadiene (TPB) and p-TerPhenyl (pTP). Both TPB and pTP are wavelength shifting chemicals that absorb vacuum ultraviolet light and re-emit light in the visible light region.

The re-emitted light is then directed toward the Silicon Photomultipliers (SiPM), which convert the photons into electric pulses. The size of the pulse is proportional to the number of incident photons.

There are three main designs which shift the wavelength and capture the light, a light trap design and two light guide designs. The light trap design, called ARAPUCA, is the baseline design for DUNE. The ARAPUCA design is a newer design, initially proposed in 2015, and has the potential for the best performance. However, since the design is newer, the earlier designs were used for the simulation.

The light guide design wavelength-shifts the photons using TPB near the surface of an optical light guide. Once shifted, the light is guided down a long, rectangular bar through total internal reflection until the photons hit the SiPMs, are absorbed, or lost. There are two light guide designs: a dip-coated and a double-shift bar. The dip-coated bars are acrylic bars which are dip-coated in TPB. The double-shift bars use commercial Wavelength Shifting (WLS) doped bars which absorb blue light and re-emit it as green. Radiator plates sprayed with TPB are layered on top of the WLS-doped bars to shift the vacuum ultraviolet light to blue light. The light guide designs are not easily scalable to the full detector.

The light trap design, named ARAPUCA and shown in Fig. 4.1, contains sixteen cells. Each cell consists of an optical window and a circuit board of SiPMs. The optical window is made

**Figure 4.1:** The ARAPUCA design during production for the prototype for DUNE before the dichroic filters were added [7].

with a dichroic filter to trap the light. The dichroic filter wavelength shifts the scintillation light using a layer of pTP. The filter is highly reflective to the shifted light but transmits the vacuum ultraviolet scintillation light. Additionally, the inside of each cell is coated with a reflective foil, further ensuring that the shifted photons are trapped within the window. The photons are measured with the SiPMs inside the light trap. The design is scalable for the full detector and has the best performance our of the three designs [5].

## 4.2 Silicon Photomultipliers (SiPM)

The photons are measured using SiPMs, which are solid state devices that use single-photon avalanche diode technology to measure single photons. In this process, the incident photon is absorbed and excites an electron from the valence band to the conduction band. The electron is accelerated with a potential difference in the SiPM. The accelerated electron knocks other electrons free in the SiPM, which creates a current. Eventually, enough electrons are knocked free to create an avalanche of electronic signal that is large enough to be measured [21].

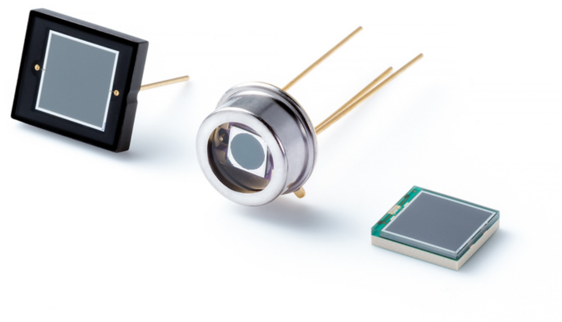

**Figure 4.2:** Three different types of Hamamatsu SiPMs used for various applications, including PET scans, scintillation detectors and Cherenkov telescopes [8].

The SiPMs must operate at $-187°$C, the boiling point of Liquid Argon. Commercially, there are two options for manufacturers of cryogenic SiPMs, Hamamatsu Photonics K.K. and Fondazione Bruno Kessler (FBK). Investigations into their performance is ongoing [5].

### 4.2.1 Dark Noise

Dark noise is the main source of noise in SiPMs. Within the active volume of the SiPM, occasionally an electron will thermally excite from the valence band to the conduction band. This electron will cause an avalanche in the same way an electron from a photon would. Most commonly, only one electron is excited. However, more rarely, multiple electrons can be excited into the conduction band, replicating a multiple photon signal. An ideal representation of dark noise is shown in Fig. 4.3. Dark noise is discussed in terms of frequency, depending on the SiPMs used.

### 4.2.2 Cross-Talk

Cross-talk is the process where a single photon triggers an additional cell on the SiPM and is measured as multiple photons. When a single photon triggers an avalanche, the electrical signal can jump to another cell on the device, resulting in a signal proportional to two photons rather than one. A typical cross-talk rate on devices like those mentioned above is 0.2 (20%) [22].

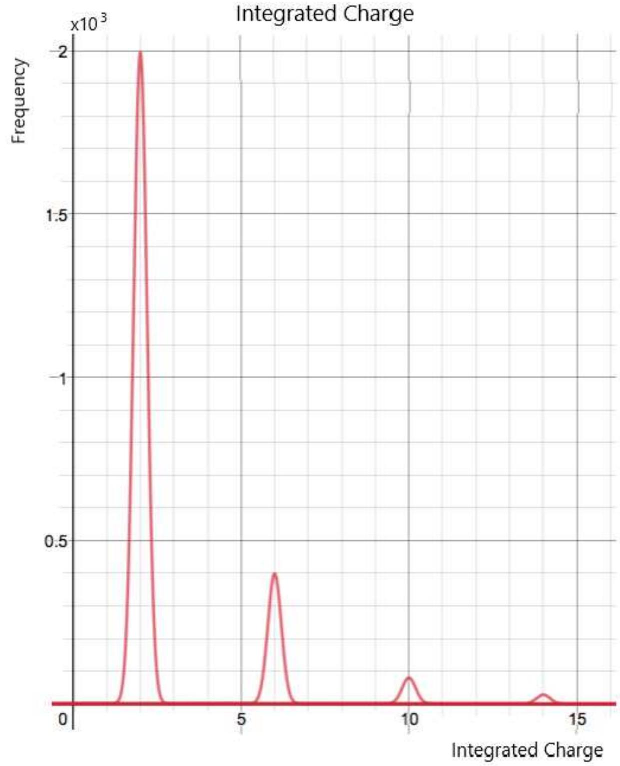


**Figure 4.3:** An ideal representation of Dark Noise. The frequency of the signal is plotted against the integrated charge of the waveform. The peaks represent different photoelectron events. The first (largest) peak is a single photoelectron event, the second peak is a double photoelectron event and so on.

### 4.2.3 Saturation

The saturation of the electronics is defined by the dynamic range. The dynamic range is the ratio of the largest and smallest signal the electronics can measure. The electronics have a dynamic range of 15 bits which means that the electronics can only measure signals smaller than 32,768 ADC counts per integration time for the input to the ADC, which is called the saturation level. At the saturation level, the measured light is no longer linearly related to the amount of light incident on the device. The signal cuts off at a constant value at and above the saturation level. When each cell on an SiPM is saturation, the signal value takes on the maximum value. The result can be seen schematically in Fig. 4.4 [22].

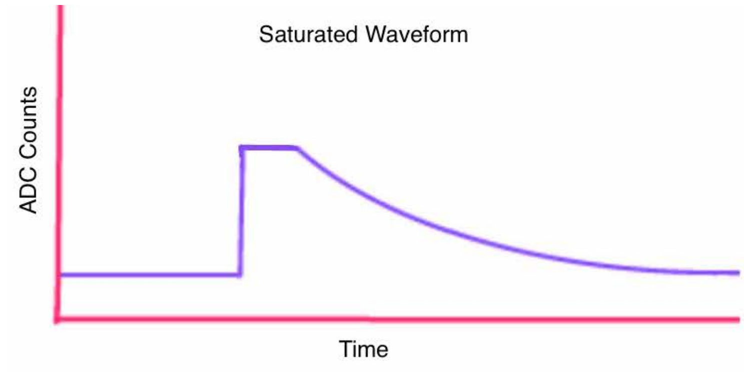


**Figure 4.4:** A waveform that passes the saturation level.

## 4.3 PDS Readout Electronics

The current prototype for the readout electronics is the SiPM Signal Processor (SSP), which digitizes electronic signals into waveforms. The SiPMs convert the photon into an electronic signal. The SSP receives the electronic signal from the SiPMs. The SSP processes the electronic signal, in the form of a voltage, and converts this into digital data. The digital data is described in units of Analog to Digital Converter (ADC) counts.

When the SSP digitizes the signal, the photon is represented by a sharp peak that decays exponentially over approximately one microsecond. The SSP only digitizes the signal if the peak of the incoming waveform is above a user-defined theshold value. A single-photon waveform is shown schematically in Fig. 4.5 [22].

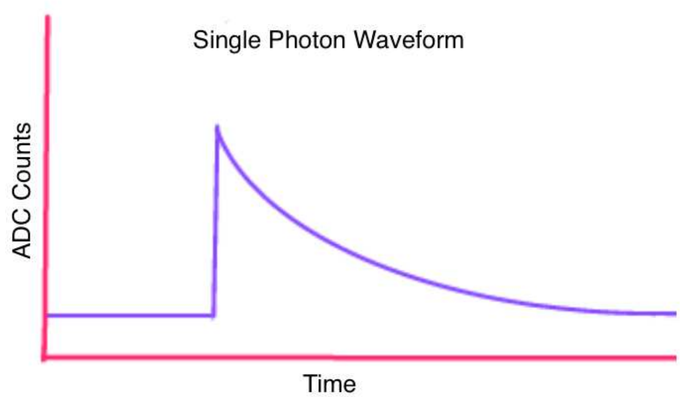


**Figure 4.5:** Cartoon of a signal digitized by the SSP.

A readout system design for the final detector has not yet been selected so multiple readout options are being investigated.

Some options for readout electronics include a charge-integration system. Charge integration electronics measure all charge within a user-selected time frame. The charge is digitized into a single number. Readout devices can store additional information such as peak height. Another option is a waveform digitizer with a lower sampling rate [5].

### 4.3.1 Line Noise

Line noise originates from electrical fluctuations in electronics rather than the photosensor. The fluctuations are distributed randomly in a Gaussian distribution around the signal. In general, line noise can be caused by power lines, motors or interference from other sources.

## 4.4 Detector Efficiency

Detector efficiency is the fraction of all photons produced that are measured by the detector. Ideally, the detector efficiency is high and the majority of photons produced are measured. However, photons can be lost in the detector at many stages.

Pure liquid argon is transparent to its own scintillation photons. However, impurities in liquid argon are not transparent. As a result, photons can be lost to the impurities in the liquid argon, reducing detector efficiency.

Wavelength shifters can fail to capture photons. For example, photons can reflect off the surfaces of the bars. Instead of getting trapped inside the light guide or trap, the reflected photons are not measured at all. Additionally, photons can transmit through both sides of the light guide and are never measured by the SiPMs. In the light trap design, photons may transmit into the trap and then transmit back out before the SiPMs measure the photon.

The number of photons measured by the PDS depends on the location in the detector. Photons are produced isotropically, and many photons will move away from the photon detectors as a result. The farther away the photons are, the lower the efficiency of the detector.

Photons are, also, lost during the SiPM measurement phase. Sometimes, once the photon is converted into an electron inside the SiPM, the electron will fail to create an avalanche. As a result, the electrical output is too small to measure. The overall detector efficiency is a combination of all the above efficiencies, as shown in Eqn. 4.1 [23].

$$\epsilon_{detector} = \epsilon_{impurity}\epsilon_{transport}\epsilon_{SiPM}\epsilon_{geometric} \tag{4.1}$$

# Chapter 5

# Simulation

The goal for the DUNE far detector simulation is to model the physics objectives for DUNE to guide the design. To do this, DUNE uses a coding framework called Liquid Argon Software (LArSoft). LArSoft is a modularized framework which simulates the detector in steps using modules. The modules simulate the particle interaction, Liquid Argon Time Projection Chamber (LArTPC), the Photon Detection System (PDS), and readout electronics. Once the particle event is simulated, the data is stored in a file and can be used in any of the other modules. LArSoft labels each event so that future modules can extract the information and use it in later stages of the simulation.

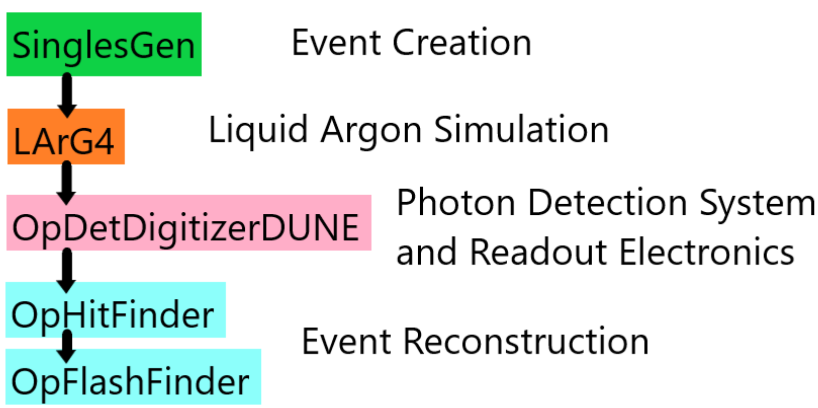


**Figure 5.1:** This figure shows the DUNE simulation chain. Each of the highlighted terms is a LArSoft module.

The PDS simulation is made up of four main stages: event creation, liquid argon simulation, PDS and readout electronics simulation, and event reconstruction, as shown in Fig. 5.1. During event creation, the particle event is created based on physics models, including direction, type of particle and energy. The liquid argon simulation models the geometry of the detector and interactions within the detector including photons produced from the recombination of electrons and the liquid argon atoms, using the information simulated during event creation. The PDS and readout electronics simulation determines the PDS response to the photons and simulates the readout electronics. The information from the electronics simulation is used during event reconstruction, which constructs event features from raw signals in the detector.

Each box in Fig. 5.1 is a module, which is a self-contained simulation code block in the framework. For example, the SinglesGen module creates single-particle events of one type. Since the code is modularized, SinglesGen can be replaced with any module that simulates events without loss of functionality. The same is true for all other modules in the list. However, since the PDS and the electronic readout system are simulated in a single module, both the PDS and readout electronics must be changed and simulated when testing different readout electronics[1].

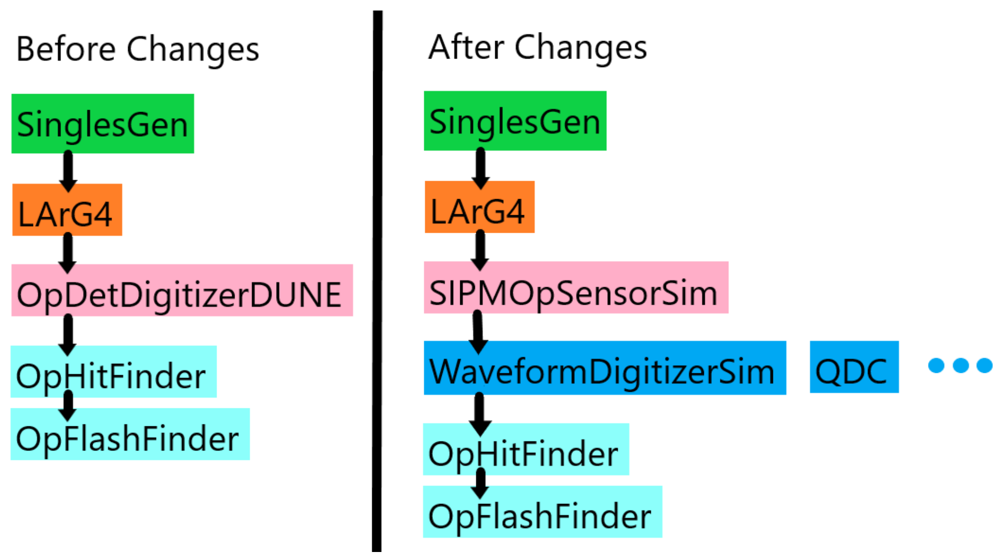


**Figure 5.2:** The changes to the code are represented above, showing each module.

To enable parallel simulation of electronic models, the PDS and readout electronics module needed to be separated into two modules. As shown in Fig. 5.2, restructuring the simulation separates the OpDetDigitizerDUNE module into the SiPMOpSensorSim and WaveformDigitizerSim modules. The SiPMSensorSim simulates the PDS and the WaveformDigitzerSim sim-

[1] This was the state of the code before the modifications

ulates waveform readout electronics. Since the WaveformDigitizerSim is a module, it can be replaced with other simulated readout electronics, such as the QDC module shown in Fig. 5.2. The readout electronics modules can then be run in parallel with each other, using simulated data from the SiPMOpSensorSim.

The Silicon Photomultiplier Simulation (SiPMOpSensorSim) implements the detector efficiencies, SiPM characteristics and thermal excitations. The readout electronics modules (WaveformDigitizerSim and QDC) simulate the readout electronics, including line noise and the photon analog signal to digital conversion.

After separating the PDS and the readout electronics modules, as shown in Fig. 5.2, different readout electronics models can be simulated in parallel. The readout electronics can be compared directly. Additionally, any number of PDS readout electronics models can be compared this way at the same time [10].

## 5.1 Configuration File

The entire simulation uses a configuration file to store various constants that include the detector efficiency and the probability of cross-talk. It further includes parameters such as the type of incoming particle and the particle's energy. These parameters can be easily changed to test various properties of the simulation.

The configuration file also defines the detector geometry. The simulation uses photon libraries based on the detector geometry to determine what photons are simulated within the detector. The photon libraries are pre-simulated libraries which simulate the detector response for photons in the detector. A full, far detector photon library is too computationally intensive to simulate. As a result, smaller subsets of the full detector are implemented in the simulation [10].

## 5.2 The Silicon Photomultiplier (SiPM) Simulation

The SiPM simulation uses information from the LArG4 (Liquid Argon Geant4) simulation. A data product, which is a container for the information created in modules, is created in LArG4 which describes the photons, including the optical detector the photon hit and the number of photons that hit. SiPMs are characterized by detector efficiency, dark noise and cross talk [10].

### 5.2.1 Detector Efficiency

The SiPM simulation applies detector efficiency, as described in Sec. 4.4. Photons are only stored by the simulation if the photon time is within the time window for the trigger. Detector efficiency is applied to the incoming photons in the time window using a random, flat distribution from 0 to 1. The detector efficiency is defined by a percentage in the configuration file. If the random number between 0 and 1 is less than this percentage, the photon is recorded [10].

### 5.2.2 Dark Noise

The SiPM simulation also models dark noise, discussed in Sec. 4.2.1, using a random exponential distribution to find the first occurrence of dark noise on an optical channel. Then, if the dark noise photon is within the trigger time frame, the photoelectron is stored. The process is repeated for the next dark noise photons on the optical channel until the end of the time window is reached. Once all dark noise is found on a single optical channel, the same process continues with the other optical channels [10].

### 5.2.3 Cross-Talk

Cross-talk, as described in Sec. 4.2.2, is simulated in the code using a random, flat distribution from 0 to 1. The probability for cross-talk is stored in the configuration file. If the random number generated is less than the probability, the single photon event is recorded as a two photons event in the output [10].

### 5.2.4 The Output Data

The SiPM simulation creates the data product OpDetDivRec. As shown in Fig. 5.3, OpDetDivRec contains the optical detector number and the photon information. The optical detector number defines the location within the overall detector. The optical detector is paired with the photon information, which contains the time of arrival (time stamp), the track ID and the number of photons simulated at that time stamp with that track ID. The time stamps of the photons are simulated to within 10 ps. The track ID is meant as an internal tool as a way to identify the photons [10].

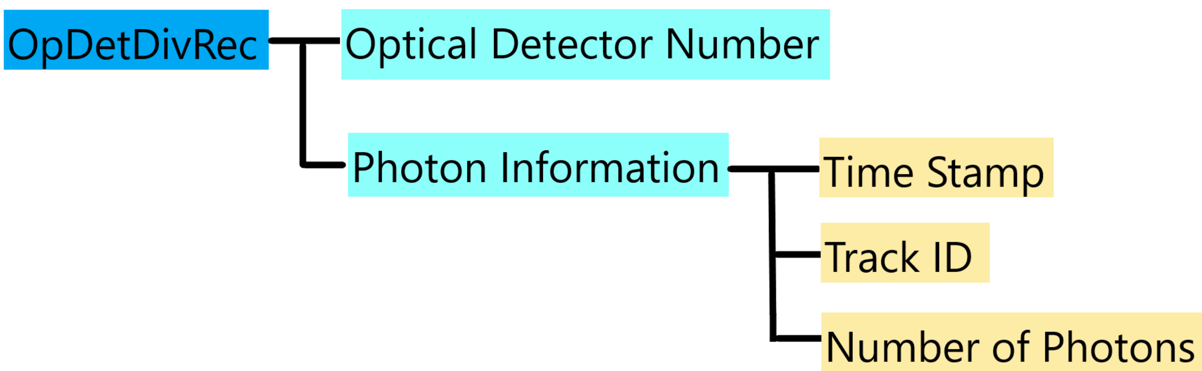


**Figure 5.3:** The OpDetDivRec data class.

## 5.3 The Waveform Digitizer Simulation

Following the electronics simulation, the output from the SiPM simulation is passed to the waveform digitizer simulation. The waveform digitizer simulation applies line noise and converts the photons into waveforms. The original electronics model included in the simulation was the SiPM Signal Processor (SSP). Prior to restructuring the simulation, the SSP was the only electronics model. After restructuring, other waveform digitizer readout models can be used [10].

### 5.3.1 Waveform Creation

As discussed in Sec. 4.3, the SSP digitizes the photons into waveforms. The simulation replicates this process. The digitized waveform of a single-photon signal is created using the peak height of the photoelectron signal and an exponential for the decay. This waveform shape is used for each photon after the photon has been digitized.

A very large vector contains all the digitized waveforms within the time window. For each simulated photon, a single-photon waveform is added to the large vector at the time of incidence, as shown in Fig. 5.4. If multiple photon waveforms overlap, the result is a superposition of the two waveforms. The vertical axis is the ADC counts stored in a time bin and the horizontal axis is time bins. For the SSP, each time bin represents 6.667 ns. Each optical channel has a large vector which stores all of the photon waveforms measured in the time window on that channel.

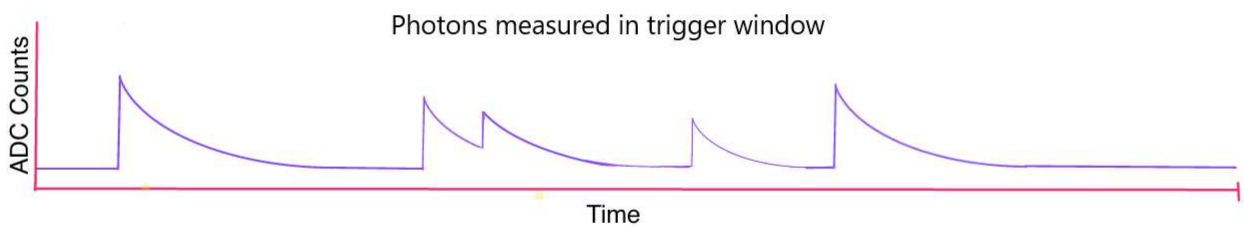


**Figure 5.4:** The vector of the time window containing the photon waveforms.

After all of the photons are digitized into the large vector, it is separated into individual waveforms. The simulation determines each individual waveforms based on their peak height. If the peak height is larger than the threshold, the individual waveform is cut off from the vector and stored. Approximately 1.5 $\mu$s of each waveform is stored after the peak and 0.2 $\mu$s before the peak [10].

### 5.3.2 Line Noise

After the photons are digitized, the line noise, as described in Sec. 4.3.1, is applied. Applying line noise to the large vector from the previous section, shown in Fig. 5.4, is computationally intensive. Therefore, line noise is added only to the portions of the vector where there are waveforms.

Line noise is added in the form of a Gaussian distribution around the mean value of 0. The width of the Gaussian depends on the PDS electronics readout model. A random number from the Gaussian distribution is added to the photon waveform at each time bin [10].

### 5.3.3 Saturation

Saturation, as described in Sec. 4.2.3, is implemented in the code after the large waveform vector is split into separate events. In the code, this is done by examining the ADC counts in the vector. If the value in a time bin is above the saturation level, the ADC count is set to the saturation level [10].

### 5.3.4 Simulation Output

The waveform digitization simulation creates the data product, OpDetWaveform. OpDetWaveform contains the photon time stamp, the optical channel, and the digitized waveform, as shown in Fig. 5.5 [10].

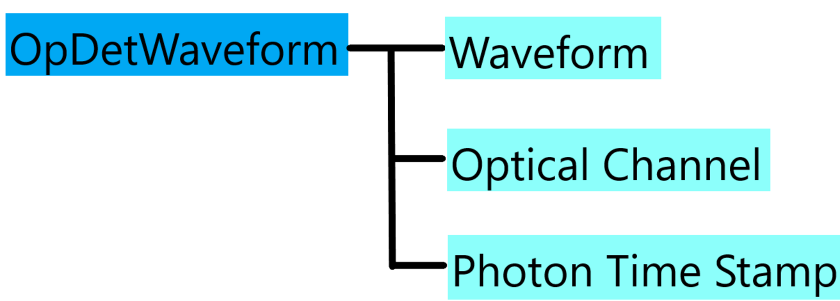


**Figure 5.5:** A cartoon representation of the OpDetWaveform class.

## 5.4 The Charge Integration Readout (QDC) Simulation

A simple electronic readout model was created to test the enhanced framework. The model is a charge integration readout system. This system triggers on an event and reads in the deposited charge within the time window. The integrated charge is simulated as a single number.

The simulation is not based on any specific commercial Charge Integration (QDC) model. It is meant to serve as a baseline which can be updated to fit specific needs [10].

The QDC and waveform digitizer simulation can be compared directly. The SiPM simulation models the data for both modules. To compare the two simulations directly, the SiPM simulation data can be stored in a file, which can be used as a source for both readout electronics modules [10].

### 5.4.1 Charge Integration

The total integrated charge is found from the waveform for a single photon. The single photon waveform is then summed over the waveform bins. Since the QDC is a toy model, the goal is to keep the hardware specifications as close to the waveform digitizer model as possible.

The simulated photons are time-ordered. All simulated photons within the readout window on a single optical channel are stored. These photoelectrons are converted into ADC counts using the integrated charge for a single photon.

A photoelectron deposits charge over a period of time. If the window ends before the photoelectron deposits all of its charge, the tail end of the pulse is cut off, as shown in Fig.5.6. All of the yellow region in Fig. 5.6 is cut off and is not recorded in the event. The event is the portion in white [10].

### 5.4.2 Saturation and Line Noise

The line noise is applied to the total integrated charge. The line noise adds a random Gaussian value around 0, with the width defined in the configuration file. The width was chosen

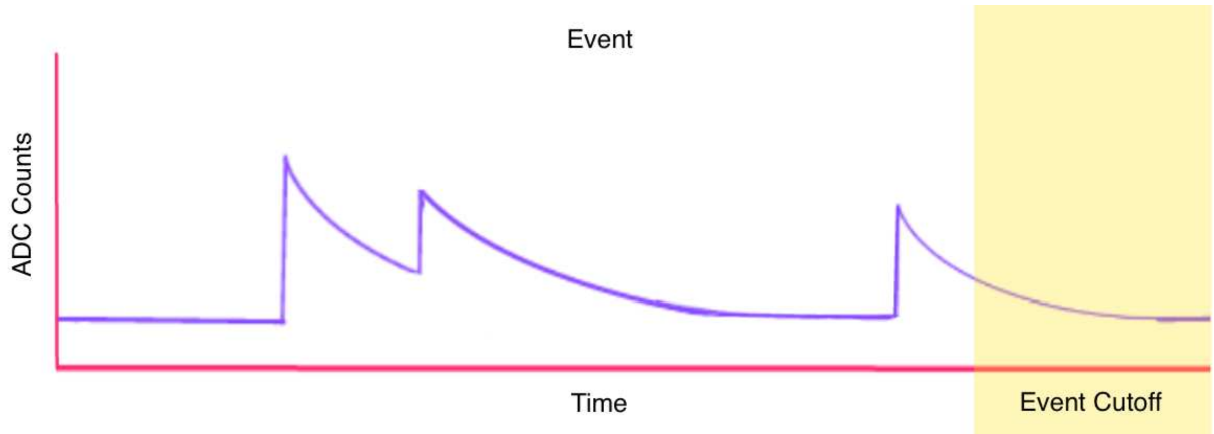


**Figure 5.6:** The waveform highlighted in yellow is cut off from the event.

to compare similarly to the waveform digitizer simulation. This value is directly added to the integrated charge.

The dynamic bit range (DBR) is defined in the configuration file. The DBR is the largest signal the system can read divided by the smallest. The saturation value (S) is found using the DBR:

$$S = 2^{DBR} - 1 \tag{5.1}$$

If the integrated charge is above this value, saturation is reached, and the output integrated charge to set to the saturation value [10].

### 5.4.3 Simulation Module Output

The QDC outputs the integrated charge within a readout window as a single number. The output also contains the optical channel and the time stamp. The data class is shown in Fig. 5.7. [10]

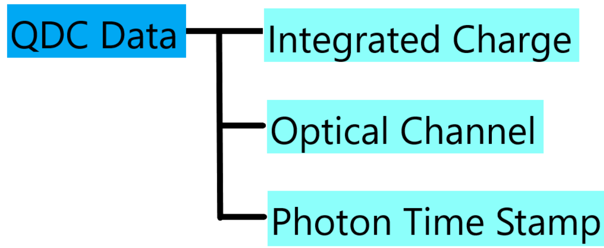


**Figure 5.7:** A graphic representation of the QDC data output.

# Chapter 6

# Analysis and Results

The PD electronics simulation is part of a much larger framework. As discussed in Chap. 5, the electronics simulation has many parts, which include the particle event simulation and detector simulation. To validate the changes made to the electronics simulation, the event creation and liquid argon simulations were run first. The event information was defined in a single configuration file that included the particle type, particle energy, the location the particle entered the detector, and many other variables.

As part of the validation process, the variables in the configuration file were changed incrementally. The majority of the variables were left unchanged, while variables of interest were varied, as discussed in later sections. The particle type, an electron, and location, $(x, y, z) = (100\text{ cm}, 200\text{ cm}, 135\text{ cm})$ shown in Fig. 6.1, were held constant throughout the studies in this chapter. The goal of these studies was to validate the changes in the simulation and that electronic readout models could run parallel to each other.

## 6.1 Running the Simulation and Detector Geometry

To run the simulation, the configuration file must be set to the desired values, including type, energy and location of the particle. The configuration file also defines the geometry of the detector, hardware efficiencies and rates, as described in Chap. 5.

The geometry used throughout the simulation is a small segment of the DUNE Far Detector, discussed in Chap. 3. The segment contains 12 APAs, as shown in Fig. 6.1. There are a total of 24 TPCs, which are APA-CPA pairs. The picture shows the lower half of the geometry, with 12 TPCs. The first outer blue layer is a layer of CPAs.

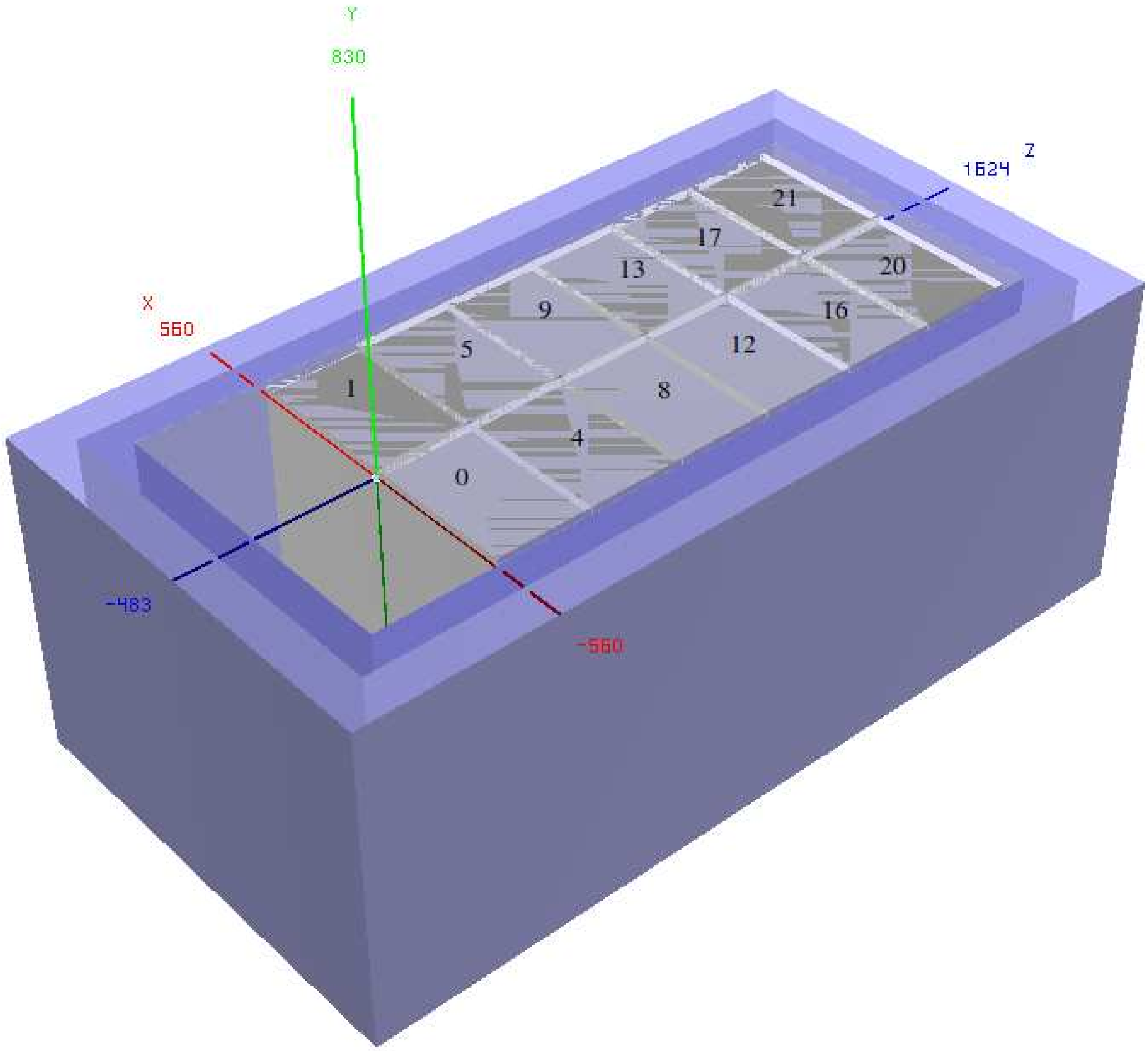


**Figure 6.1:** The lower half of the 1x2x6 detector segment of the DUNE geometry used in the simulation, showing the x, y, and z coordinates. The labelled squares are the TPCs [9].

## 6.2 Validation

The first part of the validation process was to set the input configuration file such that the dark noise, cross talk, detector efficiency and line noise did not contribute to the results. The resulting simulated data was identical. An electron was simulated in the detector, with kinetic energy of 20 MeV and located at a position of $(x, y, z) = (100\text{ cm},\ 200\text{ cm},\ 135\text{ cm})$ in the geometry shown in Fig. 6.1. This places the electron position 100 cm away from the APAs, and at the center of the TPC pair in the other dimensions. The changes to the code retained the information from the event.

Several simulations were used to validate the modified version of the electronics simulation. The first test was a comparison of the original and modified versions of the code with dark noise, cross talk, and line noise applied. The simulations were performed such that the results before and after reconstruction could be examined. The comparison is shown in Fig. 6.2.

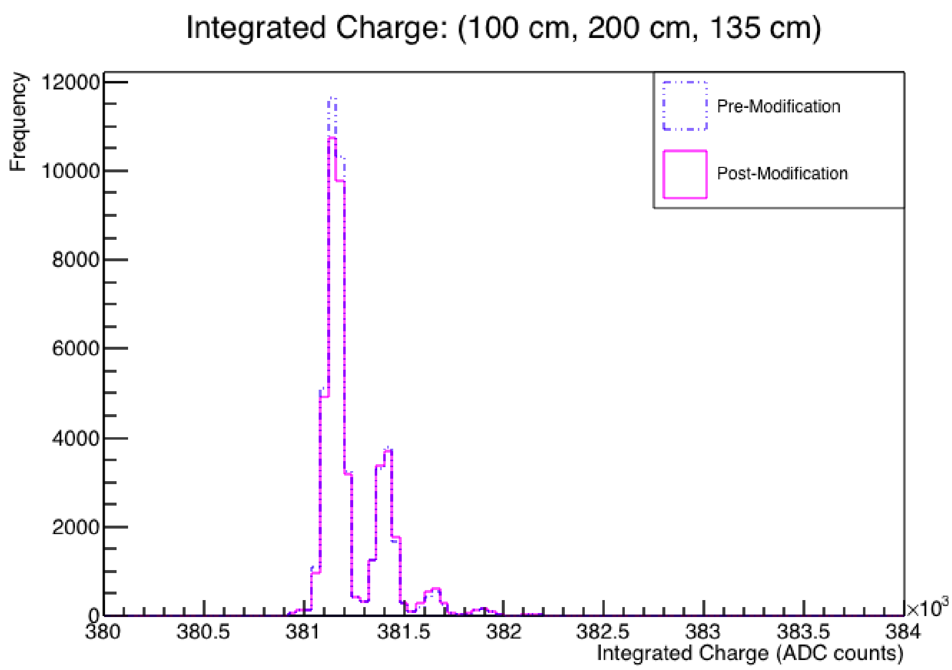


**Figure 6.2:** Integrated charge spectra for pre-modification and post-modification versions of the PD electronics simulation, using 1000 electron events in the detector. The frequency of the signal from the photon detector is plotted against the integrated charge of the waveform.

The two versions of the simulation were compared with no dark noise, cross talk or line noise. This was done to obtain a baseline of the code operation before introduction of the noise elements. As expected, these look nearly identical, as shown in Fig. 6.3. The difference between the pre-modification and post-modification graphs comes from the detector efficiency. Since the detector efficiency is random, the photons recorded differ in each run.

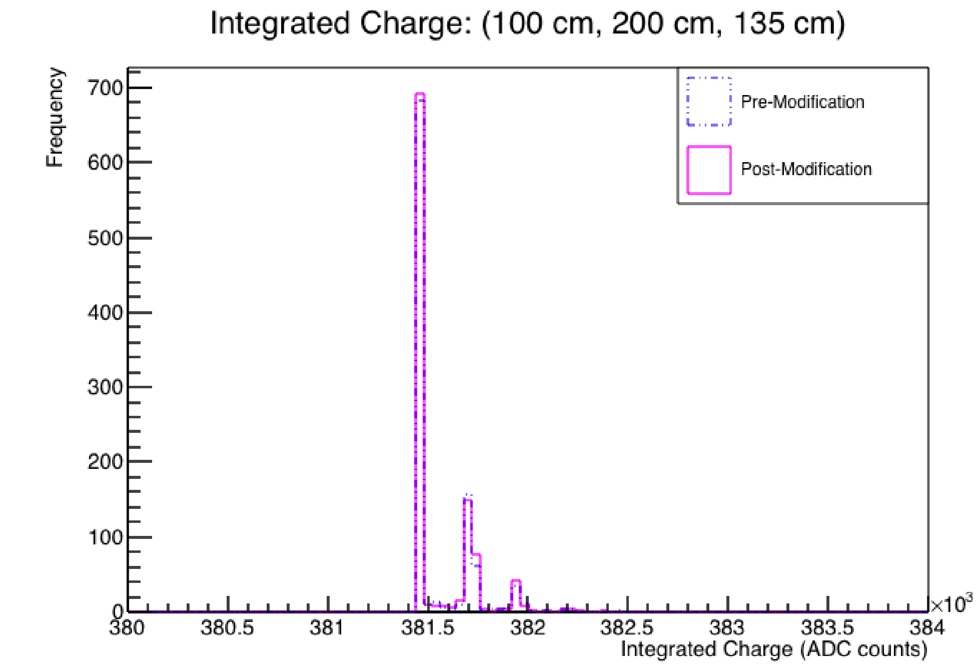


**Figure 6.3:** Integrated charge spectra for pre-modification and post-modification versions of the PD simulations without dark noise, cross talk or line noise, using 1000 electron events in the detector. The frequency of the signal from the photon detector is plotted against the integrated charge of the waveform.

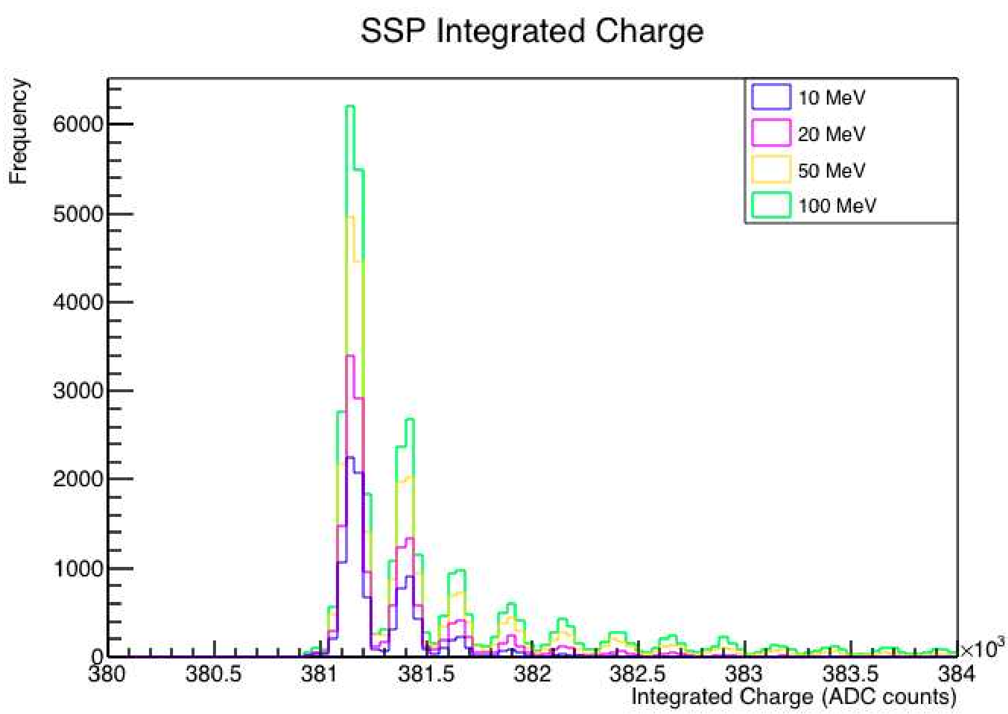


**Figure 6.4:** The effect of increased electron energy on the integrated charge, post-modification, using 1000 electron events in the detector. The frequency of the signal from the photon detector is plotted against the integrated charge of the waveform.

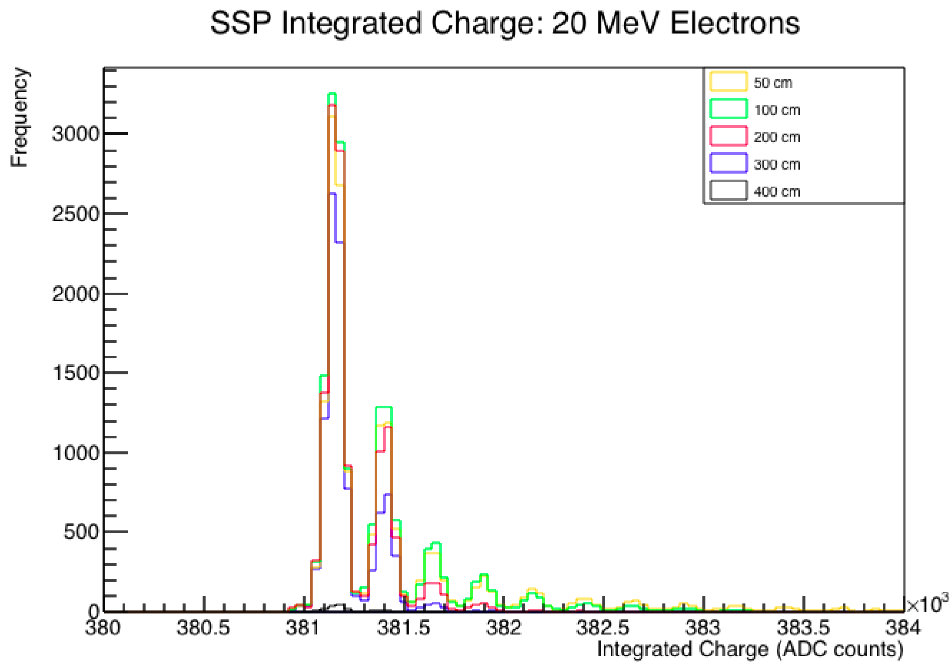


**Figure 6.5:** Integrated charge distributions for different electron starting positions, measured by distance from the APAs, post-modification, using 1000 electron events in the detector. The frequency of the signal from the photon detector is plotted against the integrated charge of the waveform.

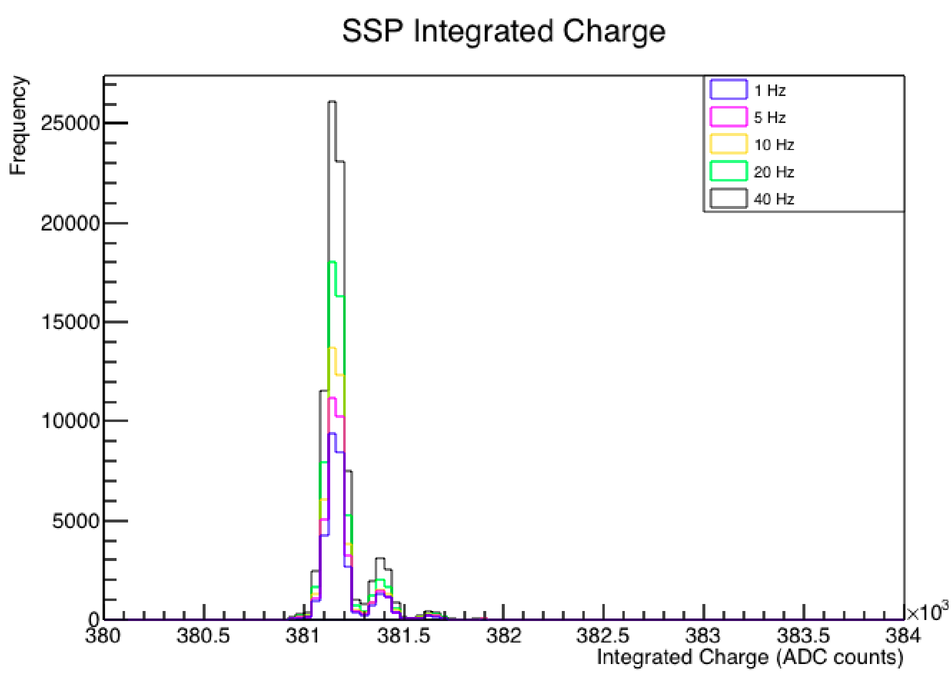


**Figure 6.6:** Integrated charge distributions for different dark noise levels, post-modification, using 1000 electron events in the detector. The frequency of the signal from the photon detector is plotted against the integrated charge of the waveform.

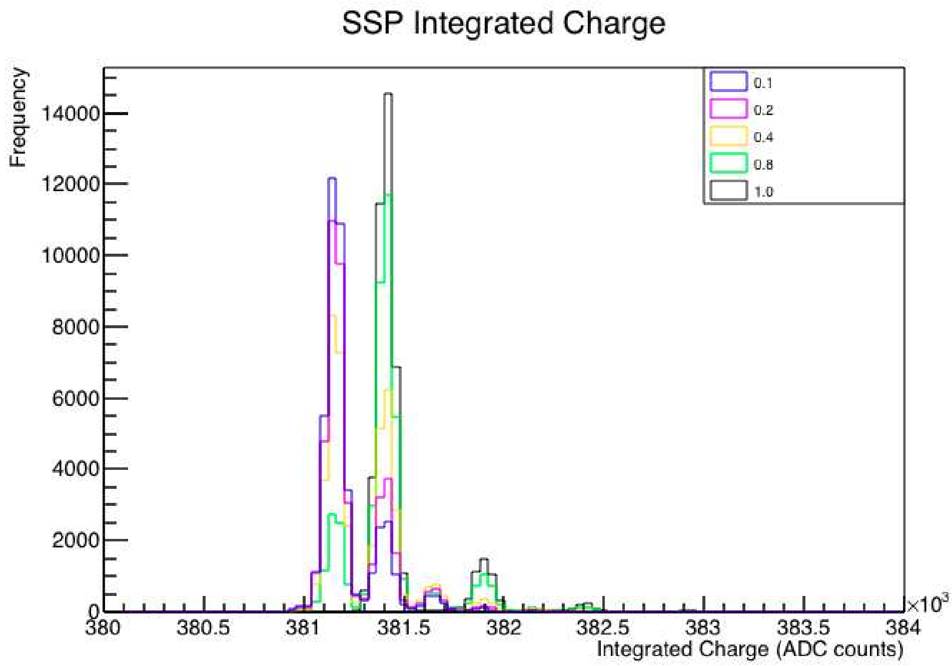


**Figure 6.7:** Integrated charge distributions for different cross-talk fractional probabilities, post-modification, using 1000 electron events in the detector. The frequency of the signal from the photon detector is plotted against the integrated charge of the waveform.

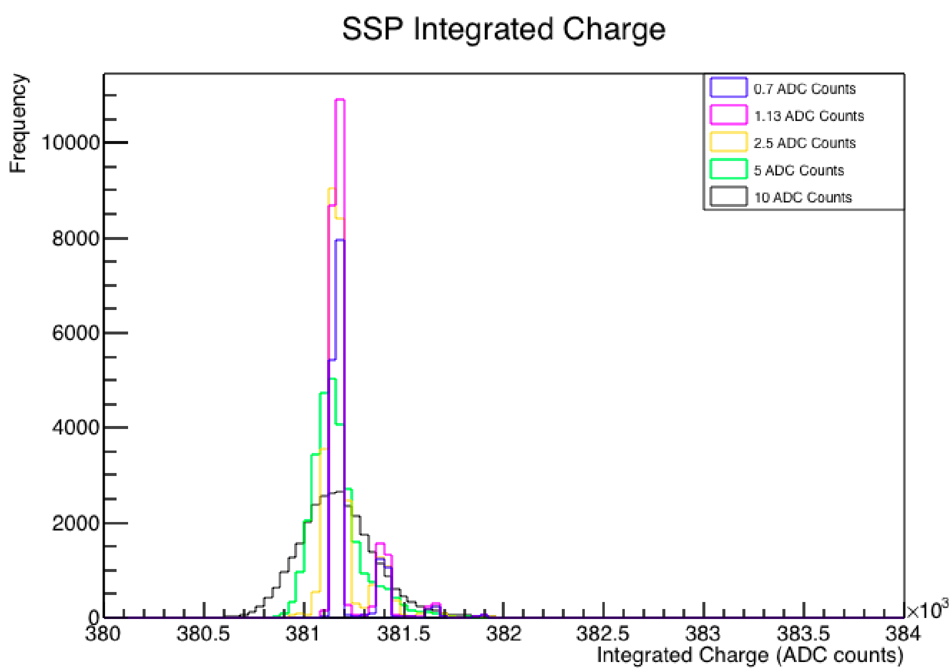


**Figure 6.8:** Integrated charge distributions for different line noise widths, post modification, using 1000 electron events in the detector. The frequency of the signal from the photon detector is plotted against the integrated charge of the waveform.

The variables in the configuration file were varied through different values to ensure that the simulation results were as expected. The energy of the electron, the position of entry of the electron, the dark noise levels, the cross talk probability, and the line noise were varied through multiple values.

**Table 6.1:** The variables changed in the simulation in order to validate their functionality.

| Variables Varied for Validation | | | | |
|---|---|---|---|---|
| Electron Energy (MeV) | Distance From APAs (cm) | Dark Noise Level (Hz) | Cross Talk Fractional Probability | Line Noise Width (ADC Counts) |
| 10 | 50 | 1 | 0.1 | 0.7 |
| 20 | 100 | 5 | 0.2 | 1.13 |
| 50 | 200 | 10 | 0.4 | 2.5 |
| 100 | 300 | 20 | 0.8 | 5 |
| – | 400 | 40 | 1.0 | 10 |

Four electron energies were used (10 MeV, 20 MeV, 50 MeV, and 100 MeV). Lower energy events would be expected to have a smaller integrated charge over the entirety of the energy spectrum, while large energy events should have a larger integrated charge over the spectrum. The results are shown in Fig. 6.4. The results are consistent with expectation.

The next step in the validation process was to vary the electron trajectory and initial position. The entry position of the event was moved from close to the APAs to a position far from the APAs. The distance from the APAs changes through the values 50 cm, 100 cm, 200 cm, 300 cm, and 400 cm, shown in Fig. 6.5. The closer the electron's starting location is to the APAs, the greater the integrated charge. The APA frame contains the PDS, so this is reasonable.

Next, the simulations were performed with five values of dark noise: 1 Hz, 5 Hz, 10 Hz, 20 Hz and 40 Hz. These values define the frequency of a dark noise event. As expected, the higher values had a larger number of dark noise events, shown in Fig. 6.6.

Cross-talk was then varied and the fractional probabilities were adjusted from 0.1 to 1.0. These values are the probability that cross talk will occur in the device. At a fractional probability of 1.0, cross talk always occurs, so there is no first peak and the second peak is much larger, as shown in Fig. 6.7. For a fractional probability of cross talk at 0.1, the second peak is much smaller and the first peak is much larger, since there are fewer cross talk events.

Line noise was tested independently from cross-talk and dark noise. The line noise Gaussian width was varied from 0.7 ADC counts to 10 ADC counts. Increasing the line noise resulted in a larger width of the peaks in the charge distributions, as shown in Fig. 6.8. A lower line noise Gaussian width of 0.7 ADC Counts has a small width, as expected.

## 6.3 Saturation

Saturation was explained in Sec. 4.2.3. When the light is digitized as a waveform, the saturation of the signals – reading the maximum digital value – results in a cutoff at the maximum value of the waveform. Fig. 6.9 shows a waveform with saturation applied. The dynamic range was set at a lower value to test saturation in this simulation. The equation for saturation uses the Dynamic Bit Range (DBR), as shown in Sec. 4.2.3. With the DBR set to 11, the maximum ADC counts for the saturation becomes $2^{10} - 1 = 1023$. The maximum ADC Count in Fig. 6.9 is 1023, as predicted. The DBR is defined in the configuration file and can be changed as appropriate.

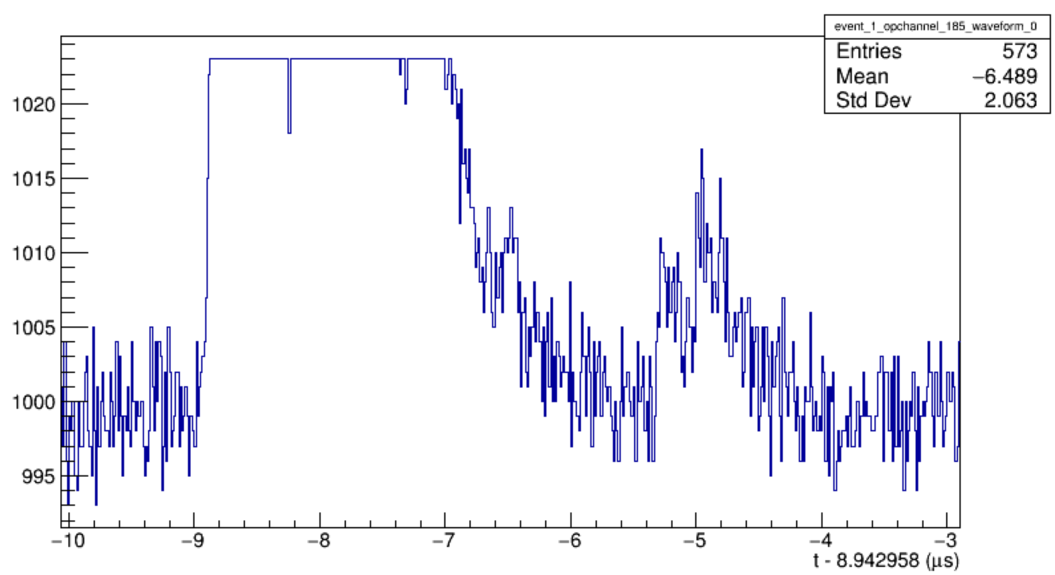


**Figure 6.9:** A simulated waveform from the SSP that has reached the saturation point.

## 6.4 QDC Results

The QDC toy model was tested in the same manner as the SSP model. The energy and starting position of the electron, the dark noise levels, the cross-talk probability, and the line noise were varied to study the effect on the simulation. The baseline simulation was an electron, with energy of 20 MeV, and a position of $(x, y, z) = (100\text{ cm},\ 200\text{ cm},\ 135\text{ cm})$, and was simulated in the same geometry. For each simulation where the variable is not discussed otherwise, the dark noise was at 10 Hz, the cross-talk fractional probability is 0.2, and the line noise was at 40 ADC counts. The table below shows the values which were varied for the QDC.

**Table 6.2:** The variables changed in the simulation in order to validate the QDC model.

| QDC Variables Varied for Validation | | | | |
|---|---|---|---|---|
| Electron Energy (MeV) | Electron Distance From APAs (cm) | Dark Noise Level (Hz) | Cross Talk Fractional Probability | Line Noise Width (ADC Counts) |
| 10 | 50 | 1 | 0.1 | 10 |
| 20 | 100 | 5 | 0.2 | 20 |
| 50 | 200 | 10 | 0.4 | 40 |
| 100 | 300 | 20 | 0.8 | 80 |
| – | 400 | 40 | 1.0 | 120 |

The first step in validating the simulation was the energy variation. The energy was varied through the values 10 MeV, 20 MeV, 50 MeV and 100 MeV. As shown in Fig. 6.10, the higher energy events have a greater integrated charge. The lower energy events have a lower integrated charge. As a note, the saturation for the QDC is what caused the peak at 384 ADC counts.

Next, the entry position for the simulated electron was varied. The distance away from the APAs was varied through 50 cm, 100 cm, 200 cm, 300 cm, and 400 cm. The results are shown in Fig. 6.11.

Dark noise was varied from 1 Hz to 40 Hz, as shown in Fig. 6.12. The higher rates of dark noise resulted in a greater number of photons. The two graphs has similar peaks, in terms of size and position. The QDC peaks are shifted downward, with the first peak starting at 380 ADC counts and the SSP starting at 381 ADC counts. The SSP uses a threshold algorithm which

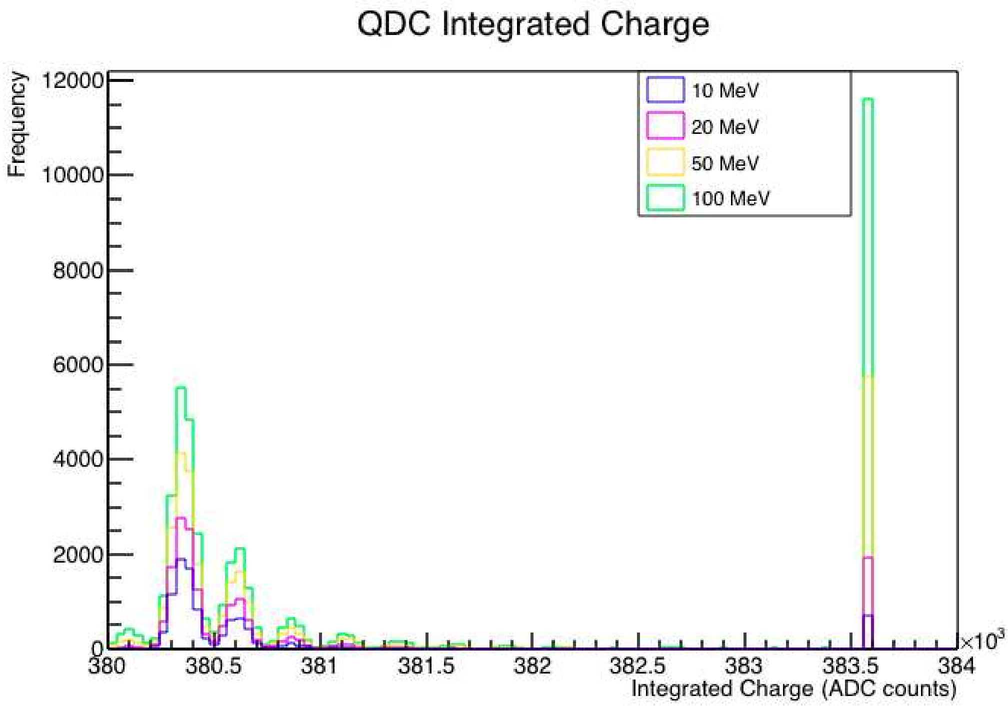


**Figure 6.10:** Integrated charge distributions for different energies, using 1000 electron events in the detector. The peak at 383.6 ADC counts is the saturation peak. The frequency of the signal from the photon detector is plotted against the integrated charge of the waveform.

records a small amount of additional points before the time window begins, resulting in the first peak beginning at 381 ADC counts. Additionally, the QDC simulation has a saturation peak at 383.6 ADC counts. The saturation for the QDC and SSP simulation work different. Whereas the SSP model cuts off the top of a waveform if it is above saturation, the QDC model can only measure integrated charge up to 384 ADC counts. When the charge deposited is above 384 ADC counts, the QDC model only measures 384 ADC counts.

Cross-talk was varied from a 10% probability to a 100% probability. As shown in Fig. 6.13, higher cross-talk probabilities resulted in smaller single photoelectron peaks and larger double photoelectron peaks in the integrated charge data. These graphs are very similar to the SSP model. Cross-talk is a part of the SiPM simulation which is the same for each electronic readout system. Therefore, cross-talk, when comparing electronic readout systems, resulted in very similar graphs.

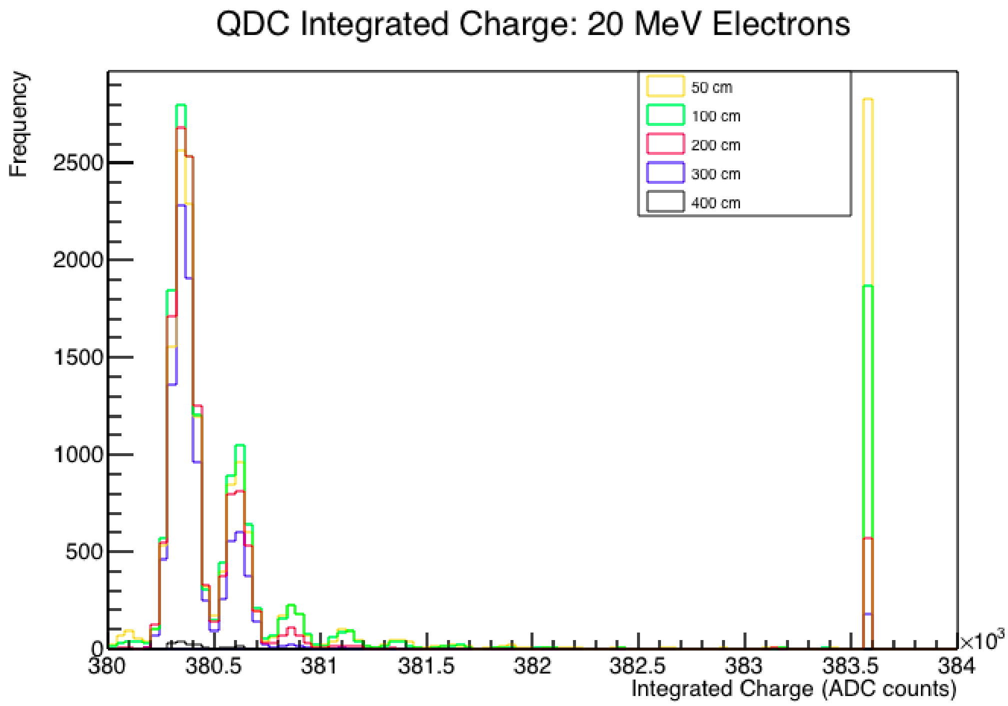


**Figure 6.11:** Integrated charge distributions for different positions, using 1000 electron events in the detector. The peak at 383.6 ADC counts is the saturation peak. The frequency of the signal from the photon detector is plotted against the integrated charge of the waveform.

The line noise was simulated in the absence of cross talk or dark noise. Line noise was varied 10 ADC counts to 120 ADC counts. Here, the line noise Gaussian width is much higher than for the SSP. These numbers were chosen to be higher for easier validation. With much lower values, the line noise variation would have been too small to see on the graph. As shown in Fig. 6.14, the line noise value changed the width of peaks. The higher line noise values resulted in larger peak widths.

Each of these simulations resulted in distributions that did not show significant deviation from those for the SSP. Increasing dark noise resulted in and increase in number of photons. When the Gaussian width of the line noise was changed, each peak in the data has the same width. Increasing the cross-talk probability increased the two photoelectron peak in the integrated charge and decreased the one photoelectron peak. When the versions were compared with and without noise, the simulated data was unchanged between versions, which verified that modularizing the code did not change the simulated data.

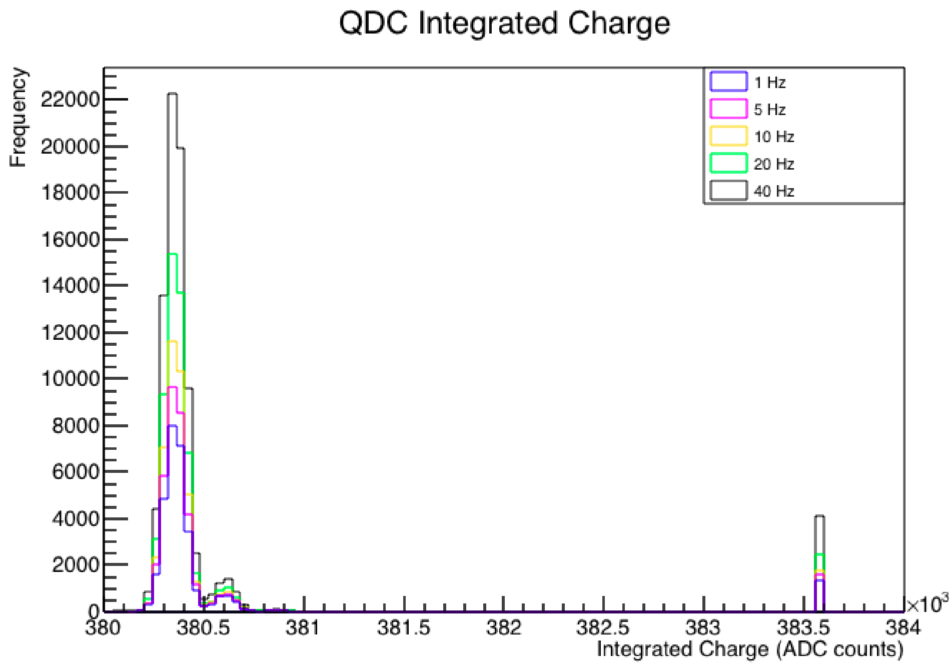


**Figure 6.12:** Integrated charge distributions for different dark noise levels, using 1000 electron events in the detector. The peak at 383.6 ADC counts is the saturation peak. The frequency of the signal from the photon detector is plotted against the integrated charge of the waveform.

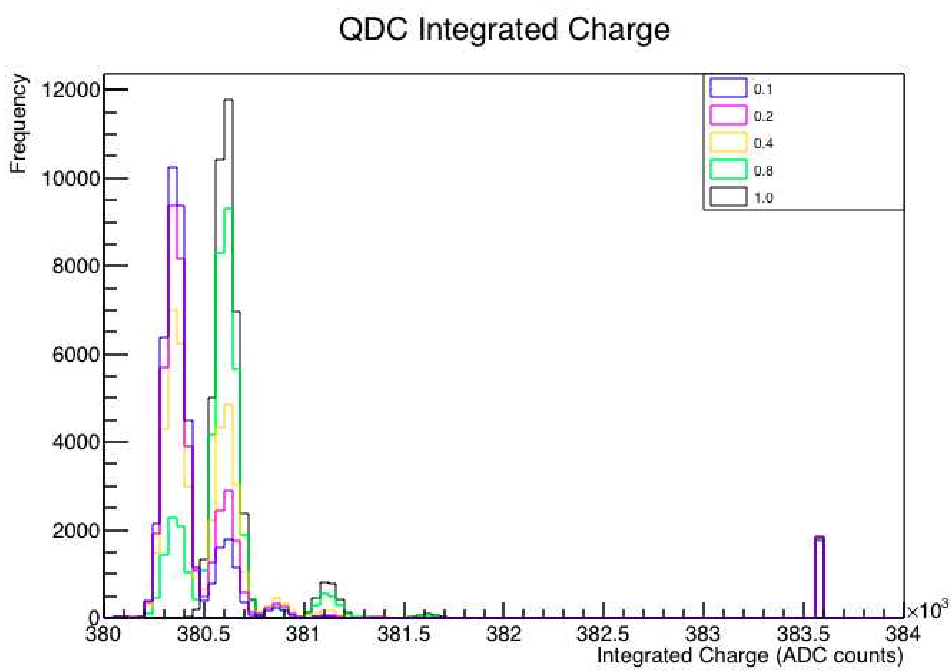


**Figure 6.13:** Integrated charge distributions for different cross talk fractional probabilities, using 1000 electron events in the detector. The peak at 383.6 ADC counts is the saturation peak. The frequency of the signal from the photon detector is plotted against the integrated charge of the waveform.

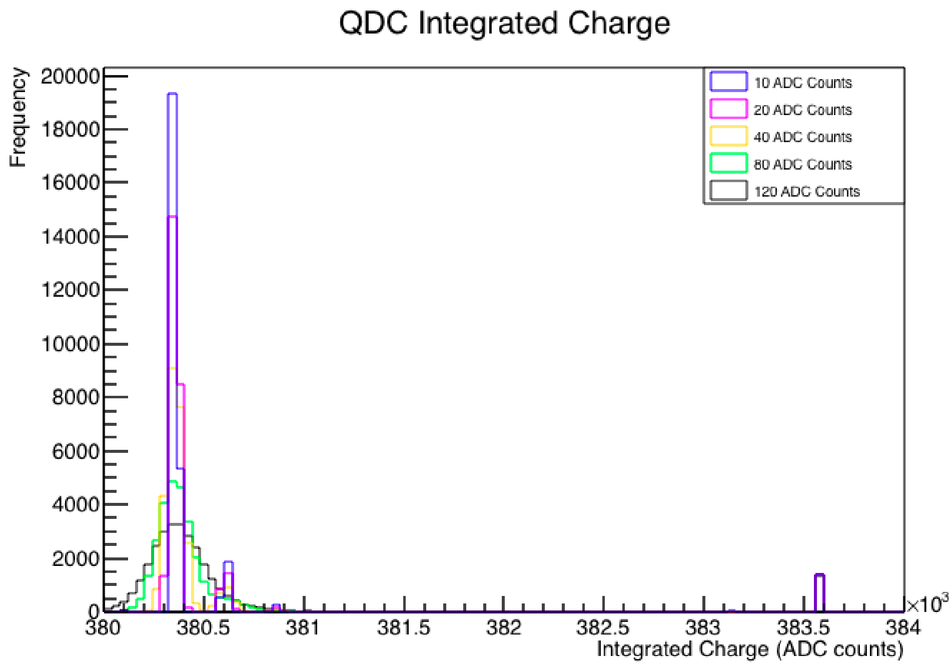


**Figure 6.14:** Integrated charge distributions for different line noise Gaussian widths, using 1000 electron events in the detector. The peak at 383.6 ADC counts is the saturation peak. The frequency of the signal from the photon detector is plotted against the integrated charge of the waveform.

# Chapter 7

# Conclusion

The DUNE electronics simulation framework was successfully modified and modularized to allow for parallel testing of readout electronics. The code was validated to ensure that the various components work as expected and that parallel testing is now possible. The code simulated the photon propagation in the event and the detector. The number of photons, the optical detector that measured the photon, and the time the photon is simulated and stored for use in later stages of the simulation, include as input to multiple modeled readout systems. The multiple readout systems can be directly compared. The framework now enables DUNE collaborators to include their own readout models in the photon detector simulation.

The information derived from the photon and electronic readout simulation is used in other modules. Future work will be done on this code, adding increased functionality, including after pulsing. Afterpulsing is when the original photoelectron causes an echo of a waveform. The data shows afterpulsing as a smaller waveform which occurs very close to the original. More robust modules will be designed to simulate possible electronic readout system for DUNE.

# Bibliography

[1] P. Hernandez. Neutrino physics. *CERN Yellow Report CERN*, pages 85–142, 2015-005.

[2] Scholberg, K. Supernova neutrinos in DUNE. Neutrino Latin America Workshop, 2016.

[3] DUNE Collaboration. The DUNE far detector interim design report volume 1: Physics, technology and strategies. *Instrumentation and Detectors*, 2018.

[4] Fermilab. Neutrino detectors. https://www.dunescience.org/neutrino-detectors/, 2019.

[5] DUNE Collaboration. The DUNE far detector interim design report, volume 2: Single-phase module. *Instrumentation and Detectors*, 2018.

[6] Fermilab. Event displays. https://microboone-exp.fnal.gov/public/approved_plots/Event_Displays.html, September 2015.

[7] CSU Lab. ARAPUCA design production pictures, June 2018.

[8] Hamamatsu Photonics K.K. MPPCs (SiPMs)/MPPC arrays. https://www.hamamatsu.com/us/en/product/optical-sensors/mppc/mppc_mppc-array/index.html.

[9] Fermilab Redmine. DUNE geometries. https://cdcvs.fnal.gov/redmine/projects/dunetpc/wiki/DUNE_Geometries, January 2020.

[10] Fermilab Redmine. DUNE computing and software. https://cdcvs.fnal.gov/redmine/projects/dune/wiki, January 2020.

[11] Mirizzi, Allessandro, et al. Supernova neutrinos: Production, oscillations and detection. *Rivista del Nuovo Cimento Vol. 39*, 2016.

[12] Brown, L.M. The idea of the neutrino. DOI: 10.1063/1.2995181, September 1978.

[13] Cowan, C. L. Jr., Reines, F., Harrison, F. B., Kruse, H. W., A. D. McGuire. Detection of the free neutrino: a confirmation. DOI: 10.1126/science.124.3212.103, July 1956.

[14] Danby, G., Gaillard, J-M., Goulianos, K., Lederman, L. M., Mistry, N., Schwartz, M., Steinberger, J. Observation of high-energy neutrino reactions and the existence of two kinds of neutrinos. *Physical Review Letters, Vol. 9*, pages 36–44, 1962.

[15] Davis Jr., R and Bahcall, J. N. Solar neutrinos: A scientific puzzle. *Science Vol. 191, Issue 4224*, pages 264–267, 1976.

[16] The SNO Collaboration. Measurement of the rate of $\nu_e + d \rightarrow p + p + e^-$ interactions produced by the $^8$B solar neutrinos at the Sudbury Neutrino Observatory. *Phys. Rev. Lett.*, pages 264–267, 2005.

[17] The Super Kamiokande Collaboration. Evidence for oscillation of atmospheric neutrinos. *Phys. Rev. Lett.*, pages 1562–1567, 1998.

[18] Griffiths, D. *Introduction to elementary particles.* John Wiley Sons, Inc., NY, USA:, 1987.

[19] Carroll, Bradley W. and Ostlie, Dale A. *An Introduction to Modern Astrophysics*, volume 2.

[20] Fermilab. How PIP-II works. https://pip2.fnal.gov/how-works/, 2013.

[21] Mascotto Massimo. Silicon photomultiplier technology at STMicroelectronics. https://indico.cern.ch/event/117424/contributions/1329247/attachments/56777/81753/STMicroelectronics_SIPM_CERN_2011-02-17.pdf, February 2011.

[22] K. Adachi, Y., Enomoto Y., Ghassemi, A., Kobayashi, K., Ohashi, Y., Sato. Technical note MPPC. https://www.hamamatsu.com/resources/pdf/ssd/mppc_kapd9005e.pdf, March 2017.

[23] Norm Buchanan. Discussion on detector efficiency. Personal Communication.